ELSEVIER

Contents lists available at ScienceDirect

Materials Today Communications

journal homepage: www.elsevier.com/locate/mtcomm





Sodium-based solid electrolytes and interfacial stability. Towards solid-state sodium batteries

Dylan A. Edelman, Taylor G. Brandt, Eleni Temeche*, Richard M. Laine

Department of Materials Science and Engineering, University of Michigan, Ann Arbor, MI 48109-2136, USA

ARTICLE INFO

Keywords: Renewable energy Sustainable Na-ion batteries Solid electrolytes All-solid-state batteries

ABSTRACT

Electrochemical energy storage is a cost-effective, sustainable method for storing and delivering energy generated from renewable resources. Among electrochemical energy storage devices, the lithium-ion battery (LIB) has dominated due to its high energy and power density. The success of LIBs has generated increased interest in sodium-ion battery (NaB) technology amid concerns of the sustainability and cost of lithium resources. In recent years, numerous studies have shown that sodium-ion solid-state electrolytes (NaSEs) have considerable potential to enable new cell chemistries that can deliver superior electrochemical performance to liquid-electrolyte-based NaBs. However, their commercial implementation is hindered by slow ionic transport at ambient and chemical/mechanical incompatibility at interfaces. In this review, various NaSEs are first characterized based on individual crystal structures and ionic conduction mechanisms. Subsequently, selected methods of modifying interfaces in sodium solid-state batteries (NaSSBs) are covered, including anode wetting, ionic liquid (IL) addition, and composite polymer electrolytes (CPEs). Finally, examples are provided of how these techniques improve cycle life and rate performance of different cathode materials including sulfur, oxide, hexacyanoferrate, and phosphate-type. A focus on interfacial modification and optimization is crucial for realizing next-generation batteries. Thus, the novel methods reviewed here could pave the way toward a NaSSB capable of withstanding the high current and cycle life demands of future applications.

1. Introduction

Advanced electrochemical energy storage systems offer great promise for storing electrical energy on a large scale for multiple applications, ranging from wind and solar farm energy storage to portable electronics and electric vehicles. [1,2] Among them, lithium-ion batteries (LIBs) have dominated the consumer electronics market since commercialization in the 1990s, offering high energy densities and long cycle lives. [3,4] However, the repeated, sometimes catastrophic, failure of LIBs — arising from degradative failure of currently used liquid electrolyte systems and/or short circuiting via dendrite growth during cycling — suggests the need for new battery systems. [5] Another important factor is the growing cost of recovering lithium from limited mineral resources. This provides additional motivation to develop alternative battery technologies using more abundant materials. [6].

Sodium-ion batteries (NaBs) are an attractive substitute for LIBs. Although Li is the most electropositive element and has a small ionic radius (-3.04~V vs. a standard hydrogen electrode, r=0.59~Å), Na is also highly electropositive ($-2.71~V,\,r=1.02~\textrm{Å}$). Intensively studied

sodium-sulfur (Na-S) [7] and sodium-nickel chloride (Na-NiCl₂) [8] batteries have been used commercially for some 30 years for energy storage at remote sites.

As projected in Fig. 1a, altering cell chemistries results in different energy storage capacities (ESP), assuming that all the resources are used to produce batteries only. The brackets show the element that limits cell production due to resource constraints. The requirements to supply world daily electricity and 1 billion EVs with an energy capability of 40 kWh each are indicated by the vertical lines. In the long run, LIB technology might not meet the demand for stationary storage and electric mobility as a result of limited resource availability (mainly Co). However, it is clear that some elements (Fe, Mn, Na, S, and C) are not critically limited, making them very attractive alternatives. [9].

The problem of material availability in LIBs is not limited to Co. The non-uniform distribution of Li metal in Earth's crust, as well as the expensive extraction and refining techniques required to recover it in pure forms, have led some to dub Li the "new gold". [10] Demand for Li resources is also expected to increase to meet future energy needs, which will be accompanied by cost increases.

Despite their lower energy densities, the fact that Na can easily be

E-mail addresses: elenite@umich.edu (E. Temeche), talsdad@umich.edu (R.M. Laine).

^{*} Corresponding authors.

Nomenclature (β-Al₂O₃) 7 Na₂O·11Al₂O₃. $(\beta''-Al_2O_3)$ 7 Na₂O·5Al₂O₃. (AM) 18 active material. (NVP) 20 Na₃V₂(PO₄)₃. (BL) 21 buffer layer. (NVZP) 19 $Na_{3-x}V_{2-x}Zr_x(PO_4)_3$. (CNF) 23 carbon nanofiber. (NZSP) 26 Na₃Zr₂Si₂PO₁₂. (CPE) 12 composite polymer electrolyte. (NBH) 36 Na₄($B_{12}H_{12}$)($B_{10}H_{10}$). (CC) 18 conductive carbon. (PIN) 23 nanoporous polymer. (NaTFSI) 26 Na(CF₃SO₂)₂N. (CE) 5 coulombic efficiency. (CCD) 15 critical current density. (PEO) 13 polyethylene oxide. (ESP) 3 energy storage capacity. (NaSSB) 4 sodium solid-state battery. (GPE) 12 gel polymer electrolyte. (NASICON) 8 sodium superionic conductor. (HV) 17 high voltage. (NaB) 3 sodium-ion battery. ionic liquid. (NaSE) 5 sodium-ion solid-state electrolyte. (IL) 21 (LAT) 17 lead acetate trihydrate. (SE) 18 solid electrolyte. (LIB) 3 lithium-ion battery. (SEI) 15 solid electrolyte interface. (NZMSP) 26 Mg-doped NASICON. (SPE) 12 solid polymer electrolyte. $(t_{\text{Na+}})$ 12 Na transfer number. (SOTA) 5 state-of-the-art. (NMTO) 29 $Na_{0.44}Mn_{0.67}Ti_{0.33}O_2$. (SN) 36 succinonitrile.

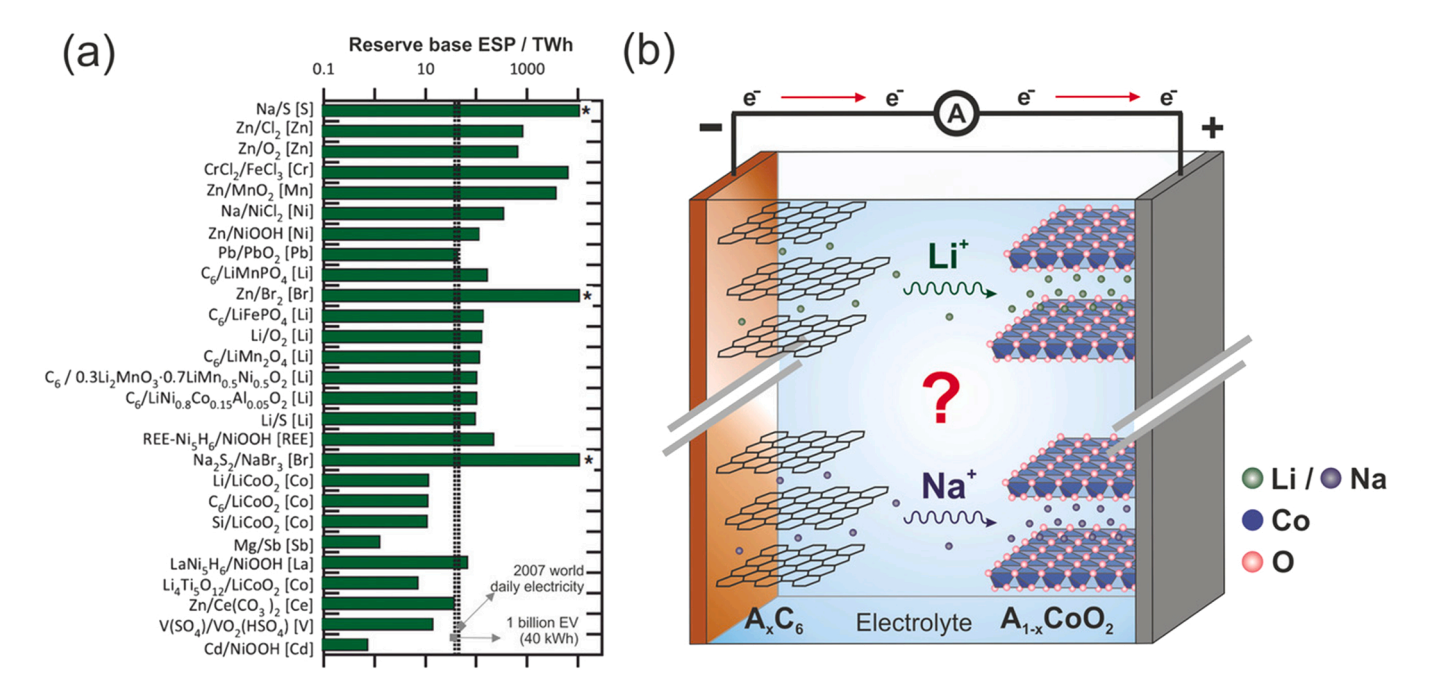


Fig. 1. (a) Reported energy storage potential for various battery chemistries. The limiting element due to resource constraints is listed in brackets. ESP values that are beyond the limit of the Figure are indicated by a star. (b) Sketch of conventional LIB cell with graphite anode and $LiCoO_2$ cathode. The working principle is the same for NaBs and LIBs but NaBs have an increased mobile ion size.

(b) Reprinted with permission from Nayak et al. [9]. Copyright 2018 Wiley.

recovered from seawater suggests that NaBs could be a sustainable alternative to LIBs with decreased raw materials costs. [11] However, conventional NaBs also use organic liquid electrolytes and suffer problems similar to current LIBs. [12,13] Thus, low thermal stability, flammability, a limited electrochemical window, and electrolyte leakage hinder their large-scale use due to safety concerns similar to those associated with LIBs. [14,15].

Solid electrolytes are a compelling solution for alleviating many of these problems. Sodium solid-state batteries (NaSSBs) are thus potential candidates to complement LIBs to fulfill future energy storage needs. Plus, they will allow use of sodium metal anodes and therefore could offer high energy and power densities. [16] NaSSB performance can therefore be expected to depend highly on the performance of the solid-state electrolyte.

For example, cell thermodynamic stability is governed directly by the electrochemical stability window of the electrolyte, [17] which significantly influences electrochemical performance and battery life. [18] The development of state-of-the-art (SOTA) NaSSBs mandates solid-state electrolytes with enhanced ionic conductivities, superior electrochemical and thermal stabilities, and wide electrochemical operating windows. [19].

Although superionic conductivity ($>10^{-3}~{\rm S~cm^{-1}}$) at ambient temperature has been realized for sodium-ion solid-state electrolytes (NaSEs), there are other issues that must be improved further before realizing a battery with high coulombic efficiency (CE) and long cycle life that can also withstand the current densities necessary for practical applications. These problems include the chemical compatibility of electrodes with electrolytes, charge transfer rates at interfaces, unstable

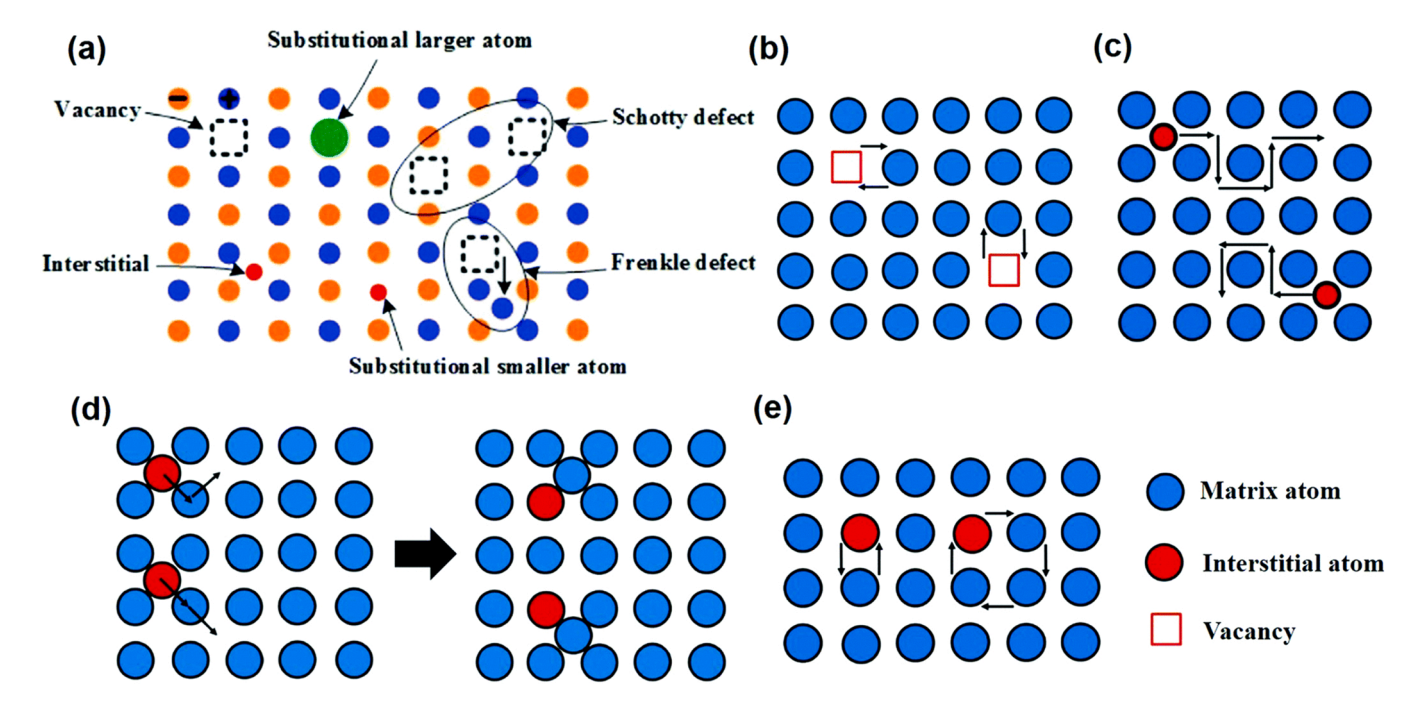


Fig. 2. Schematic of common point defects (a) and ion migration mechanisms in crystalline solids via (b) vacancy, (c) direct interstitial, (d) knock-off, and (e) direct exchange and ring. [34].

(a) Reproduced/Adapted from ref. [34] with permission from the Royal Society of Chemistry, Copyright 2020.

mechanical contacts at interfaces, and the chemical or volumetric changes that occur coincident with ${\rm Na}^+$ (de)intercalation.

Numerous reviews have summarized the development, synthesis, and electrochemical properties of various NaSEs. Detailed, comprehensive reviews of NaSE performance in this context can be found elsewhere. [16,19–29] The focus of this review is to consolidate fundamental electrochemical properties of NaSEs with their resulting performance in symmetric-, half-, and full-cells. Additionally, this paper provides a thorough review of recent publications that demonstrate novelty in improving interfacial performance in NaSSBs.

We review here the various types of NaSEs classified based on their ionic conduction mechanisms and crystal structures. The electrochemical performance and properties of key NaSEs are discussed. In addition, methods for improving the chemical, electrical, and mechanical stability of NaSSB interfaces are assessed: including anode wetting, solution processing, and co-sintering. The stability of electrode/electrolyte pairs based on design principles and strategies, along with mechanisms to improve interfacial contact, are summarized. These methods are further analyzed in the context of cathodes and catholytes. Finally, we propose future research directions and address key challenges that must be overcome for successful commercial implementation of NaSSBs.

2. Transport mechanisms in NaSEs

The optimization and design of superior Na^+ conducting materials must rely on a fundamental knowledge of ionic transport mechanisms in inorganic and polymer electrolytes. This is the first focus of this review.

2.1. Mechanisms of Na+ transport in inorganic NaSEs

Battery designs targeting NaSEs that function in demanding applications favor the use of inorganic materials, [30,31] as they are expected to offer good chemical, thermal, mechanical and electrochemical stabilities. Such NaSEs must also offer high ionic conductivity and low electronic conductivity. As a general rule, inorganic NaSEs provide mobile Na⁺ ions residing in locally symmetrical structures. [32] Their

ionic conduction mechanism(s) depend primarily on defect type-s/concentrations, numbers of mobile ions, and energy barrier(s) to diffusion. [32,33].

In point defect diffusion mechanisms, Na^+ ions hop from one site to an adjacent one within a locally crystalline framework, wherein diffusion rates are controlled by the availability of vacancy/interstitial sites (Fig. 2a). [34] Systems that function via vacancy mechanisms (Fig. 2b), must offer small ion-hopping lattice strains, thereby reducing activation energy barriers.

Transport mechanisms depending on point defects can only be effective with control of vacancy concentrations, distance between adjacent vacancy sites, and the electrostatic environment along the diffusion trajectory. [12].

Interstitial diffusion mechanisms (Fig. 2c) allow Na $^+$ ions to move either directly to available interstitial sites, or via a "knock-off mechanism," (Fig. 2d) wherein they repel a neighboring ion and simultaneously cause it to migrate to an adjacent interstitial site. Fig. 2e demonstrates direct exchange and ring mechanisms.

2.1.1. Oxide-based NaSEs

In the 1970 s, fields such as solid-state science and electrochemistry received increased attention following the discovery of ion-conducting properties in selected solid structures. [35–38] The beta alumina structure was considered a promising ionic conductor as early as 1967 due to its low electronic conductivity. [31] Indeed, commercially viable Na/S and Na/NiCl $_2$ ZEBRA batteries are a direct result of this early interest. [7] Unfortunately, operating conditions for beta alumina systems mandate elevated temperatures (>300 $^{\circ}$ C) to ensure optimal ionic conductivity, which limits battery energy densities due to encapsulation requirements and increased electrolyte thicknesses. [39].

There are two beta alumina polymorphs: $\beta\text{-}Al_2O_3$ and $\beta\text{''}\text{-}Al_2O_3$. $\beta\text{-}Al_2O_3$ has a hexagonal structure with $P6_3/mmc$ symmetry, [31] whereas $\beta\text{''}\text{-}Al_2O_3$ has a rhombohedral structure with R_3m symmetry. The main differences are the chemical stoichiometry and stacking sequences of oxygen ions across the conduction plane. $\beta\text{-}Al_2O_3$ (Na₂O·11Al₂O₃) is a layered structure with alternate spinel-structured alumina blocks and conduction planes as shown in Fig. 3a, while the

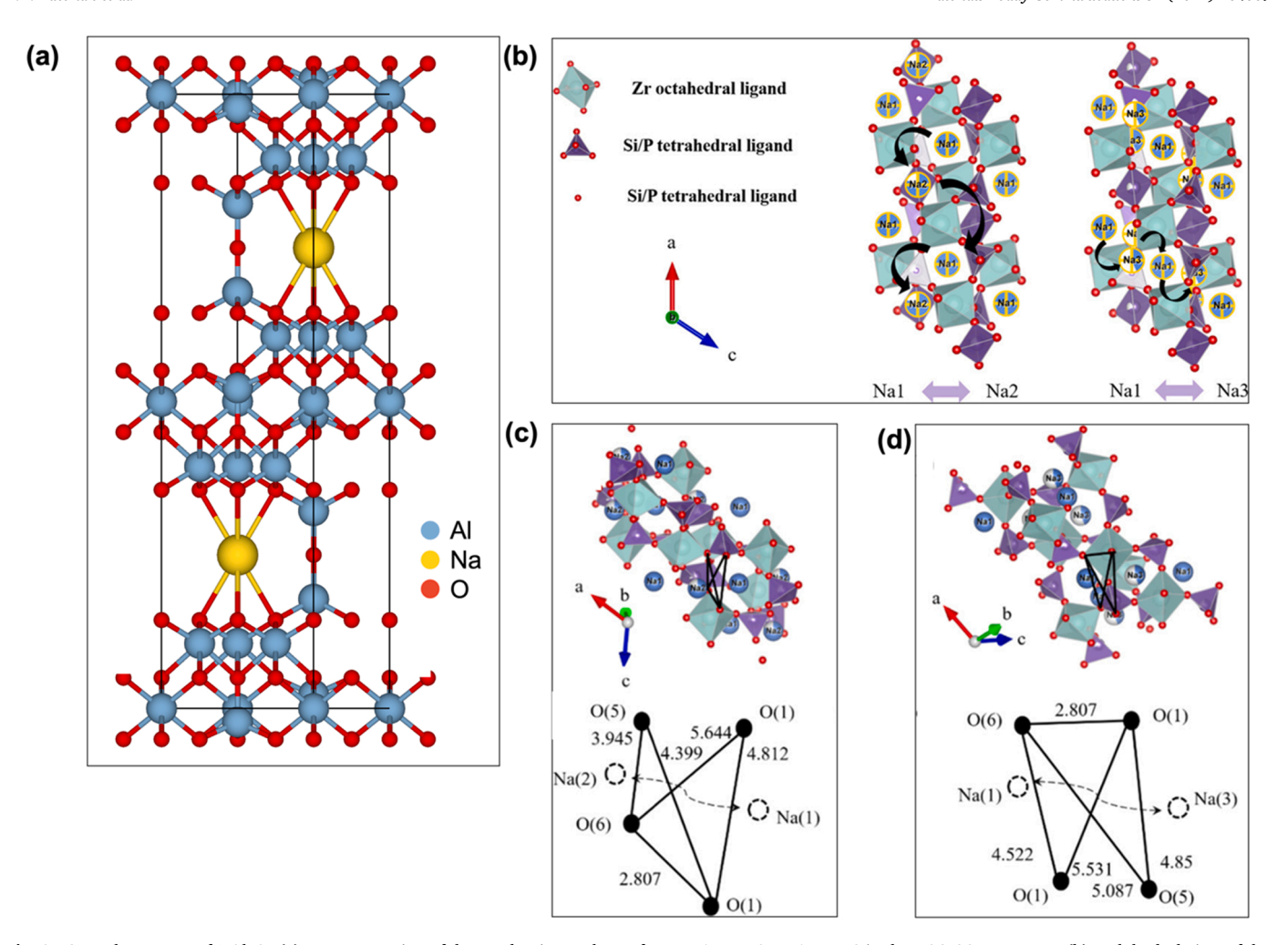


Fig. 3. Crystal structure of β -Al₂O₃ (a). Representation of the conduction pathway from Na1 to Na2; Na1 to Na3 in the NASICON structure (b). Polyhedral view of the T1, T2 bottlenecks from Na(1) to Na(2) (c) and From Na(1) to Na(3).

(d) Reprinted (adapted) with permission from Liu et al. [43] Copyright 2020 American Chemical Society.

Table 1Reported ionic conductivities for several oxide-based NaSEs.

Electrolyte	Prototype	Processing Method	Sintering schedule	σ (S cm ⁻¹) / Temp. (°C)	Activation Energy (kJ mol ⁻¹)	Ref.
$\beta' \prime - Al_2O_3$	Y ₂ O ₃ (0.5 wt%)	Double zeta process/ BM/C	1450°C / 4 h	3.48 × 10 ⁻² / 300	-	[45]
	MgO (0.4 wt%)	SR / BM	1500°C / 2 h	0.137 / 300	25.6	[46]
	TiO ₂ (2 wt%) and ZrO ₂ (10 wt%)	LF-FSP	1320°C / 2 h	$5.4 \times 10^{-6} / 25$	_	[41]
NASICON	Ba _{0.05}	SR / BM	1260°C / 16 h	$1.2 \times 10^{-3} / 25$	_	[47]
	Ca _{0.05}	SR / BM	1260°C / 16 h	$2.1 \times 10^{-3} / 25$	_	
	Sr _{0.05}	SR / BM	1260°C / 16 h	$1.8 \times 10^{-3} / 25$	_	
	Mg _{0.05}	SR / BM	1260°C / 16 h	$3.5 \times 10^{-3} / 25$	24.1	
	La _{0.3}	SR / BM	1225 ℃ / 15 h	$6.7 \times 10^{-3} / 25$	_	[48]
	Y _{0.2}	SR / BM	1225 ℃ / 15 h	$4.3 \times 10^{-3} / 25$	_	
	Ca _{0.1}	SG	1250 °C / 5 h	$1.67 \times 10^{-3} / 25$	28.0	[49]

 $\textbf{C} = \text{calcination} \mid \textbf{BM} = \text{ball-milling} \mid \textbf{SR} = \text{solid-state reaction} \mid \textbf{SG} = \text{sol-gel} \mid \textbf{LF-FSP} = \text{liquid feed flame spray} \mid \textbf{NASICON} = \text{Na}_{3+(2)x} \text{Zr}_{2-x} \text{M}_x \text{Si}_2 \text{PO}_{12} \text{Nasicon} = \text{Na}_{3+(2)x} \text{Zr}_{2-x} \text{M}_x \text{Nasicon} = \text{Na}_{3+(2)x} \text{Zr}_{2-x} \text{Zr}_{2-x} \text{M}_x \text{Nasicon} = \text{Na}_{3+(2)x} \text{Zr}_{2-x} \text{Zr}_{2-x} \text{Nasicon} = \text{Na}_{3+(2)x} \text{Zr}_{2-x} \text{Z$

two conducting layers of β "-Al₂O₃ (Na₂O·5Al₂O₃) are separated by three spinel blocks. [40].

 $\beta^{"}\text{-}Al_2O_3$ has been the subject of multiple studies prompted by its higher ionic conductivity than $\beta\text{-}Al_2O_3$ (Table 1). [31,41,42] This higher ionic conductivity is attributed to the high Na $^+$ concentration in the conduction plane. Compared to polycrystalline materials, single crystal $\beta^{"}\text{-}Al_2O_3$ offers four times higher ionic conductivity (1 S cm $^{-1}$ at 300 °C). [31] Unfortunately, processing single crystals is not cost-effective at

industrial scales. [12] Thus, numerous efforts have been made to optimize the conductivity of polycrystalline $\beta^{\prime\prime}\text{-Al}_2O_3$. In particular, the introduction of dopants (Li⁺, Mg²⁺, Mn⁴⁺, Ti⁴⁺) or addition of secondary phases (Y₂O₃, ZrO₂, TiO₂) are reported to be effective methods of modifying the $\beta^{\prime\prime}\text{-Al}_2O_3$ structure by providing mechanical strength, reducing or preventing excessive grain growth, and improving Na⁺ conductivity. [31].

Processing pure β"-Al₂O₃ is still challenging due to coincident

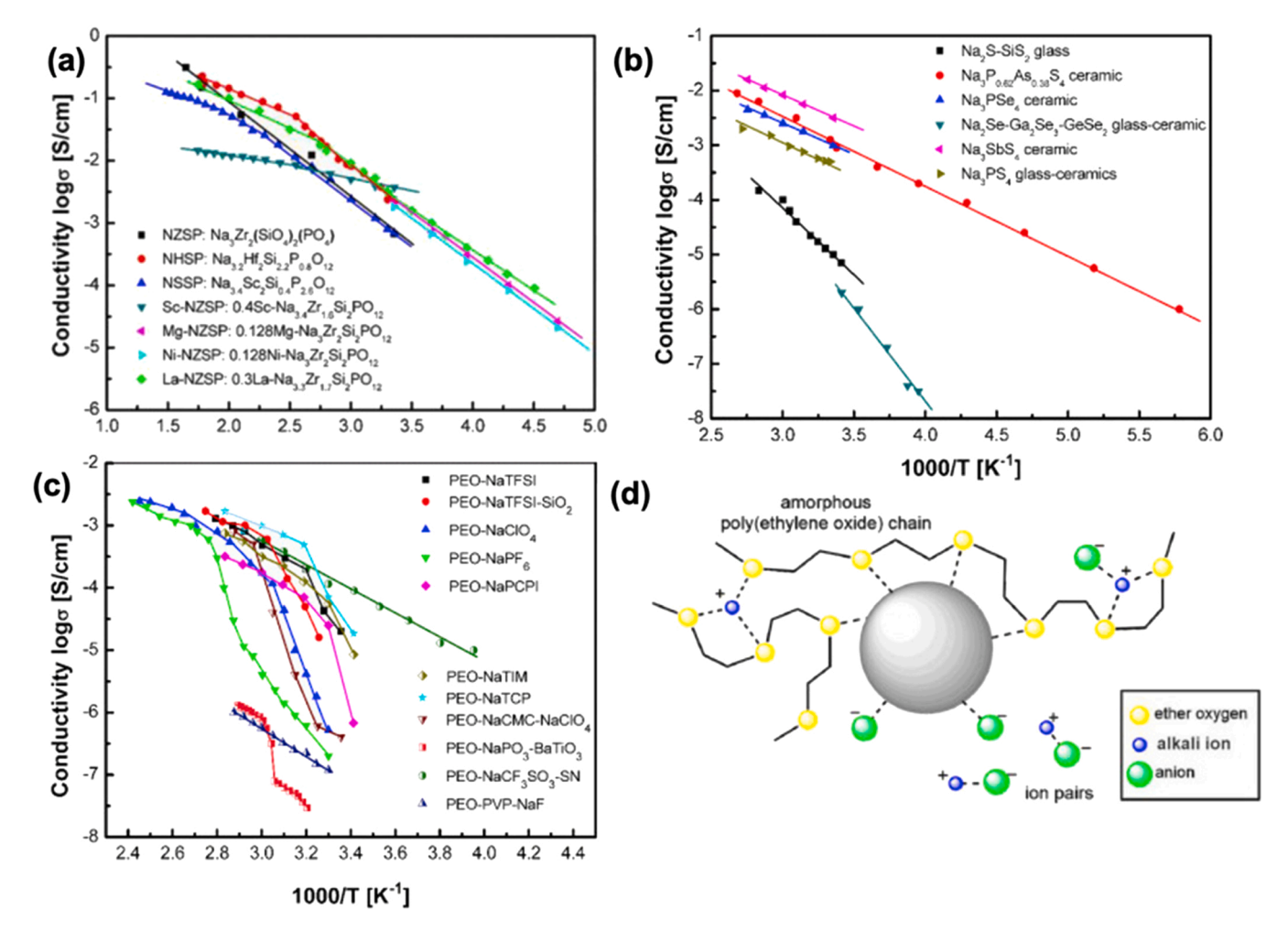


Fig. 4. Conductivities of various (a) oxide, (b) sulfide and (c) polymer NaSEs. (d) schematics of ionic conduction mechanism within PEO polymer and alkali salt. (c)Reprinted from [12]. Copyright 2019, with permission from Elsevier

formation of β -Al₂O₃ and NaAlO₂ secondary phases, which react readily with CO₂ and H₂O, reducing chemical stability at ambient. [41] The moisture-sensitive nature of β -Al₂O₃ affects both processing and storage considerations. [12] Furthermore, ionic conduction pathways within both β -Al₂O₃ and β "-Al₂O₃ are limited to 2-D as Na⁺ ion diffusion proceeds only within the conduction planes, limiting their utility in NaSSBs.

Goodenough et al. [37] first demonstrated Na⁺ conduction in the sodium superionic conductor (NASICON) family of compounds in 1976. Today, the NASICON structure is well recognized as a promising material for NaSEs, with a wide electrochemical window (0–5 V) and high ionic conductivity attributed to 3D Na⁺ diffusion paths (see Table 1). [12.41].

NASICON materials, with a general formula $Na_{1+X}M_2Si_{3-X}PO_{12}$ (0 < x < 3), also present two polymorphs – rhombohedral and monoclinic – depending on the sodium content. [44] NASICON materials offer 3D ionic conductivity through interconnected tunnels constructed from mixtures of (Si/P)O₄ tetrahedra and ZrO₆ octahedra as shown in Fig. 3b. [43].

The monoclinic phase (1.8 < x < 2.2) is stable at ambient and transforms to the rhombohedral form above $150\,^{\circ}\text{C}$. In Fig. 3b, Na sites Na1, Na2, and Na3 [43] denote the path(s) whereby Na⁺ hopping occurs. Diffusion is limited by bottleneck diameters (Fig. 3c-d), labeled as T1 with a smaller and T2 with a larger cross-section. While the highly symmetrical structure of rhombohedral NASICON offers a lower diffusion activation energy, [12] monoclinic NASICON facilitates better Na⁺ migration due to its larger bottleneck cross-section (Table 1).

Numerous studies have shown that the electrochemical properties of

the NASICON framework can be optimized by aliovalent doping of M or P/Si sites to enhance Na $^+$ mobility (Fig. 3). [32] Zhang et al. [50] demonstrated that La $^{3+}$ doped NASICON generates secondary phases (Na $_3$ LaPO $_4$) $_2$ that promote densification and improve the chemical composition at grain boundaries, improving bulk and grain boundary conductivities from 2.0 to 4.5 mS cm $^{-1}$ for pristine vs. doped polycrystalline analogs, respectively.

Song et al. [47] reported that doping NASICON with Mg enlarges the bottleneck diameter, thereby lowering the activation energy and enhancing ionic conductivity. As the conductivity of polycrystalline material depends on both grain and grain boundary conductivities, significant efforts have targeted decreasing grain boundary resistance, lowering impurity concentration, and improving final densities. Table 1 and Fig. 4a compare the total conductivities of different NASICON electrolytes synthesized via solid state reactions, sol-gel, or spray pyrolysis methods.

The main limitations of oxide-based NaSEs arise from high impedance and unstable interfaces at ambient. [32,51] Studies have shown that Na metal dendrites often occur via uneven Na plating at the surface and grain boundaries of NASICON electrolytes, causing short-circuits. [52,53] Efforts to improve interfacial impedance are discussed in Section 3.

The search for alternatives to oxide NaSEs led to efforts to develop sulfide-based electrolytes because sulfur is less electronegative than oxygen and thus binds Na⁺ less strongly, providing faster diffusion processes.

 Table 2

 Reported ionic conductivities for several sulfide-based NaSEs.

Electrolyte	Composition	Processing Method	σ (S cm ⁻¹) / Temp. (°C)	Activation Energy (kJ mol ⁻¹)	Ref.
NPS	Na ₃ PS ₄	SR / BM	$4.6 \times 10^{-4} / 25$	19.0	[54]
	$Na_3P_{0.62}As_{0.38}S_4$	BM	$1.46 \times 10^{-3} / 25$	24.7	[55]
NSbS	c-Na ₃ SbS ₄	SR / BM	$2.8 imes10^{-3}$ / 25	5.79	[63]
	Na ₃ SbS ₄	SR	$1.1 imes10^{-3}$ $/$ 25	19.3	[58]
	Na _{3.02} (Sb _{0.98} Sn _{0.02})S ₄	AQ	$2 imes 10^{ ext{-4}}$ / 25		[61]
NMPS	$Na_{10}GeP_2S_{12}$	_	$4.7 \times 10^{-3} / 25$	19.3	[64]
	$Na_{10}SnP_2S_{12}$	BM	$4 \times 10^{-4} / 25$	34.3	[59]
	$Na_{11}Sn_2PS_{12}$	SR	$3.7 \times 10^{-3} / 25$	37.3	[60]
S substitution	Na ₃ PSe ₄	SR / BM	$1.16 \times 10^{-3} / 25$	20.3	[62]
	$Na_{2.9375}PS_{3.9375}Cl_{0.0625}$	SR	$1.14 \times 10^{-3} / 30$	24.0	[65]

 $\textbf{BM} = \textbf{ball-milling} \mid \textbf{SR} = \textbf{solid-state} \; \\ \textbf{reaction} \mid \textbf{AQ} = \textbf{aqueous} \; \\ \textbf{solution} \mid \textbf{NPS} = \textbf{Na}_3 \\ \textbf{PS_4} \mid \textbf{NSbS} = \textbf{Na}_3 \\ \textbf{SbS_4} \mid \textbf{NMPS} = \textbf{Na}_{(10+x)} \\ \textbf{M}_{(1+x)} \\ \textbf{P}_{(2-x)} \\ \textbf{SpS}_{(2-x)} \\ \textbf{SpS}_{(10+x)} \\ \textbf{M}_{(10+x)} \\ \textbf{M}_{(10+x)$

2.1.2. Sulfide-based NaSEs

Unlike oxides, sulfide-based NaSEs form good interfacial contacts between electrolytes and electrodes attributed to their malleable nature. [19] In addition, sulfide-based NaSEs are accessible via low-temperature synthesis routes and can easily be cold-pressed onto electrodes, which minimizes production cost. [19].

 Na_3PS_4 is the most often studied sulfide NaSE attributed to its high ambient ionic conductivity and wide electrochemical window. [54,55] Na_3PS_4 exhibits high ionic conductivity (2–4.6 $\times 10^{-4}$ S cm⁻¹) with low activation energy (19–27 kJ mol⁻¹) due to intimate contact between grains that decreases grain boundary resistance. [19,56,57] Na^+ conductivity can also be enhanced by aliovalent substitutions. Thus, superionic conductivity at ambient (10^{-3} S cm⁻¹) is observed for tetragonal Na_3SbS_4 . [58] Despite these advantages, Na_3PS_4 is incompatible with common electrodes, as described in Section 4.1.

Sn-doped sulfide solid electrolytes have also been explored. [59,60] However, unit cell volumes were found to decrease with increasing Sn concentration in some systems as a result of electrostatic attraction. [61] This decreases the bottleneck size for Na⁺ diffusion, which also decreases conductivity. Likewise, S can be replaced either partially or fully with dopants (Cl, Se). Replacement of S with Se, for instance, was found to increase Na₃PS₄ conductivity due to the higher polarizability of Se and a larger unit cell size. [62].

Table 2 and Fig. 4b list several relevant ionic conductivities of various sulfide-based NaSEs reported in the literature. For a description of the processing methods presented in Tables 1 and 2, please see Supporting Information Section S1.

Sulfide-based NaSEs offer high ionic conductivities at ambient and facilitate intimate contact between the electrode and electrolyte; however, they are moisture sensitive and have poor thermal stabilities, hindering their application on large scales. [12] In addition, reaction with humidity generates toxic H_2S gas which complicates manufacturing and recycling efforts. Further studies to alleviate these challenges by either modifying the NaSE composition/structure, or by introducing surface coatings, are needed. This could broaden the selection of viable inorganic NaSEs capable of operating at ambient for use in commercial products.

2.1.3. Complex hydride and halide electrolytes

Orimo's group first reported on complex hydride NaSEs in 2012. These complex hydrides (NaBH₄, NaNH₂, NaAlH₄, and Na₃AlH₆) exhibit high ionic transfer numbers ($t_{\rm Na+} \sim 1$). [66] However, the ambient ionic conductivities were only 2.1×10^{-10} and 6.4×10^{-7} S cm⁻¹ for NaAlH₄ and Na₃AlH₆, respectively. In a subsequent study, Orimo's group demonstrated a slightly higher ambient ionic conductivity (3×10^{-6} S cm⁻¹) by combining NaBH₄ and NaNH₂ at a molar ratio of 1:1, forming Na₂(BH₄)(NH₂) with an antipervoskite-type structure. [67].

Complex hydrides with larger anions (i.e. $Na_2B_{12}H_{12}$, $Na_2B_{10}H_{10}$) demonstrate high ionic conductivity of 0.1 S cm⁻¹ at 300 °C due to their cation-vacancy rich structure at elevated temperatures. [68] However,

the phase transition-temperature is too high for most practical applications. Numerous ongoing efforts seek to lower this temperature via anion modifications, crystallite disordering, and anion mixing. [69,70].

The full replacement of hydrogen by halogens NaMX (M= Zr, Y, Er; X=Cl, Br, I) paved the way for halide-based NaSEs with ionic conductivities similar to sulfides and stabilities comparable to oxides. [71, 72] These compounds have received growing interest due to their high ambient ionic conductivity (1 mS cm $^{-1}$) and large voltage stability (\sim 4 V) owing to the halide anionic framework. [73] The fast-conducting diffusion pathway is enabled by the monovalent nature of halogens resulting in weaker interaction with Na $^{+}$ ions. Although halide-based NaSEs have optimal electrochemical performance, they are typically moisture sensitive and have poor low potential stability. Hence, future work must address these challenges via surface modification, coating, and doping.

2.2. Polymer electrolytes

Solid polymer electrolytes offer several advantages over inorganic NaSEs such as enhanced resistance to variations in electrode volumes during cycling, excellent flexibility, and low-cost processing. [74,75] In addition, dendrite growth may be suppressed in solvent-free polymers under certain conditions. [76] Substantial efforts have targeted elucidation of ion transport mechanisms in polymer electrolytes. In this section, polymer-based electrolytes are divided into solid polymer electrolytes (SPEs), composite polymer electrolytes (CPEs), and gel polymer electrolytes (GPEs).

2.2.1. Solid polymer electrolytes

SPEs typically consist of sodium salts dissolved in polymer matrices. [77,78] Polyethers dissolve Na-salts by ether oxygen complexation of Na $^+$ as found in LIB analogs. [79,80] Thus, polyethylene oxide (PEO)-based SPEs have received considerable attention because of their superior ability to solvate Na $^+$; combined with segmental motion, this allows for rapid Na $^+$ transport near their Tg of 65 $^\circ$ C. In addition, high purity PEO is commercially available with different molecular weights and at low cost. [76].

SPEs typically offer low ionic conductivities at ambient $(10^{-7}-10^{-6} \text{ S} \text{ cm}^{-1})$, which is a significant barrier to commercialization. [81] The ionic conduction mechanism is affected by two factors: one is the fraction of the amorphous material in the polymer matrix, and the other is T_g . It is generally accepted that Na⁺ transport (diffusion) occurs preferentially in amorphous regions of solid PEO. [76] Significant efforts to improve SPE ionic conductivities have focused on reducing crystallinity. [82,83] Such efforts include modifying the polymer matrix by copolymerization, crosslinking, blending, increasing salt concentrations, and immobilizing the anions as pendant groups. [76].

In general, SPEs are bi-ionic conductors; [76] that is, both the cations and anions are mobile, greatly reducing transference numbers (generally < 0.5 due to electro-polarization from anion buildup). [76]

 Table 3

 Reported ionic conductivities for composite polymer electrolytes.

Туре	SPE/salt	Filler	σ (S cm ⁻¹)/ Temp (°C)	Ref.
SPE	PCL-PTMC/NaFSI	-	1.64×10^{-5} / 25	[88]
CFPM	PEO and PPC/NaN (SO ₂ CF ₃) ₂	$Na_3Zr_2Si_2PO_{12}$	1.2×10^{-4} / 25	[89]
	PEO/NaTFSI	$Na_{3.4}Zr_{1.8}Mg_{0.2}Si_2PO_{12}$	2.8 × 10 ⁻³ / 80	[75]
			6.0×10^{-5} / 30	
	PEO/NaFSI	Na _{3.4} Zr _{1.8} Mg _{0.2} Si ₂ PO ₁₂	2.4 × 10 ⁻³ / 80	[74]
			4.4×10^{-5} / 25	
	PEO/NaCF ₃ SO ₃	NaTi ₂ (PO ₄) ₃	3.0 × 10 ⁻⁵ / 40	[90]
CFPF	PEO/NaClO ₄	Na ₃ Zr ₂ Si ₂ PO ₁₂	2.1×10^{-5} / 30	[91]
	PVDF-HFP	$\beta' \prime - Al_2O_3$	7.13×10^{-4} / 25	[92]

 $\begin{array}{ll} \textbf{PCL-PTMC} &= polyester-polycarbonate \ copolymer \ | \ \textbf{NaFSI} = sodium \ bis(fluorosulfonyl) \ imide \ | \ \textbf{NaTFSI} = Na(CF_3SO_2)_2N \ | \ \textbf{PEO} = polyethylene \ oxide \ | \ \textbf{PPC} = polyester \ | \ \textbf{PVDF-HFP} = poly \ (vinylidene \ fluoride-co-hexafluoropropylene) \ | \ \textbf{SPE} = solid \ polymer \ electrolyte \ | \ \textbf{CFPM} = ceramic \ filled \ polymer \ matrix \ | \ \textbf{CFPF} = ceramic \ framework \ polymer \ filler \\ \end{array}$

Electro-polarization typically leads to a decrease in the overall electrochemical performance due to high internal resistance, voltage losses, and dendritic growth. [84].

To minimize polarization and increase Na⁺ transference numbers, anion mobility must be reduced – either by anchoring the anions to the polymer backbone or adding chelating agents that preferentially bind anions. [76] Multiple attempts to improve the ionic conductivities of SPEs are reported in the literature through the addition of plasticizers, polymer blends, and ceramic fillers (TiO₂, SiO₂, and ZrO₂). [75,85,86]

All are designed to interfere with crystallization and thereby promote Na⁺ mobility. The introduction of solids is addressed separately below.

2.2.2. Composite polymer electrolytes

The addition of ion-conducting ceramic oxides to SPEs to form composite polymer electrolytes has been shown to increase ionic conductivity (Table 3). Ceramic fillers also act to increase the thermal and electrochemical stability of SPEs as well as Na⁺ transference numbers. [87] These fillers can be incorporated in SPEs in two ways: as ceramic particles mixed into a polymer matrix (ceramic filled polymer matrix, CFPM) or as a continuous ceramic framework filled with polymer (ceramic framework polymer filler, CFPF). [74] Table 3 lists selected CPE conductivities.

The introduction of ceramic to a SPE increases ionic conductivity due to the addition of new ion migration channels along the surface and through the bulk of the ceramic. [92] In addition, the incorporation of ceramic particles breaks up local polymer crystallinity, allowing for increased chain percolation and faster ionic conduction. NASICON-type compounds are common active fillers in CPEs owing to their high ionic conductivity. [50,91] More broadly, oxide-type NaSEs are preferable for CPE fillers as opposed to sulfides due to their higher stability and lower moisture sensitivity. [93,94] Although polymer chain mobility is increased by these ceramics, most CPEs only offer reasonable ionic conductivities above room temperature or with added liquid electrolyte (Table 3). [75,94,95].

The current SOTA solid-state CPE has cross-linked $\beta'\prime-Al_2O_3$ nanowires and a poly (vinylidene fluoride-co-hexafluoropropylene) matrix with an ambient ionic conductivity of 0.7 mS cm $^{-1}$. [92] Since ceramic fillers can improve thermal stabilities to ≈ 150 °C, elevated operating temperatures are possible. [74] For these reasons, CPEs often demonstrate superior cycling stability in electrochemical cells than SPEs (see Section 4.3).

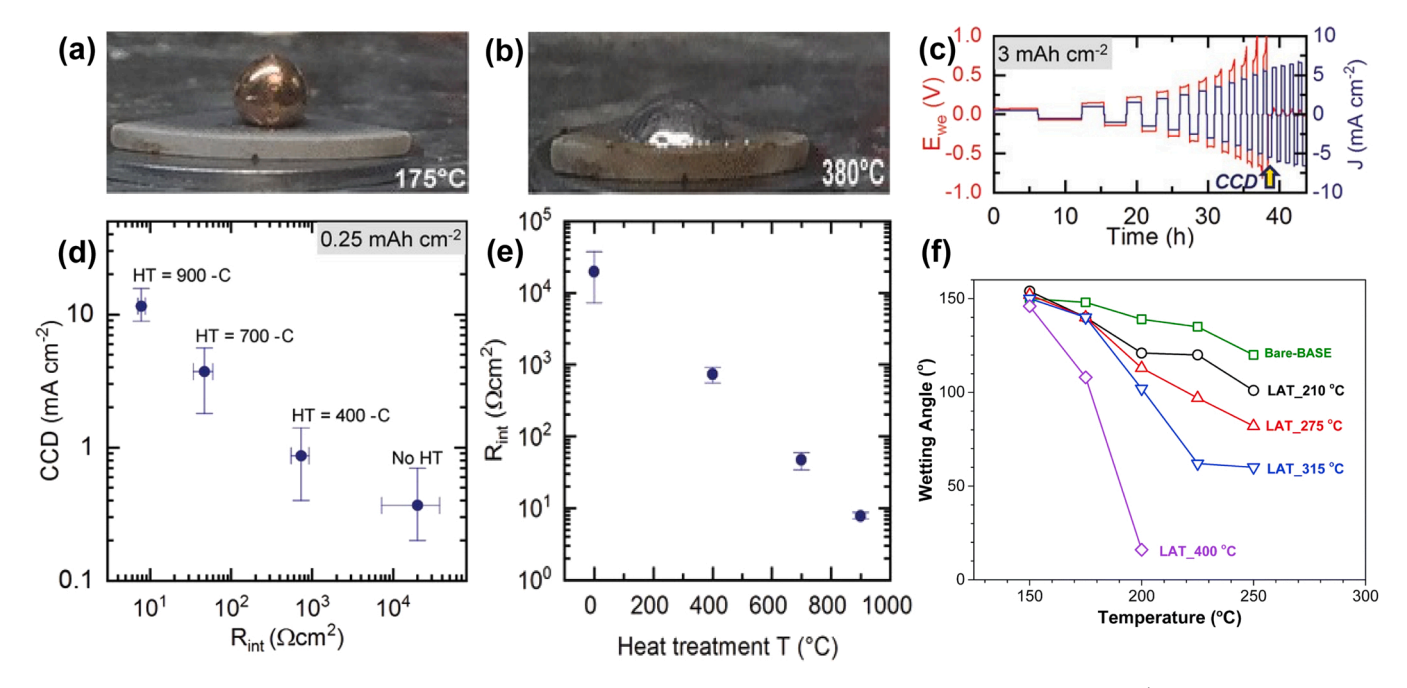
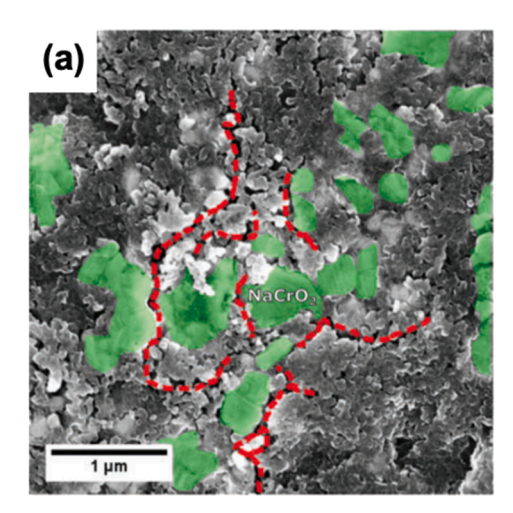


Fig. 5. Examples of Na metal wetting onto NASICON electrolyte pellet at (a) 175 °C and (b) 380 °C. (c) Potential response of Na/Na- $\beta'i$ – Al_2O_3 /Na cell undergoing CCD measurement at 5 mA cm⁻². (d) CCD as a function of interfacial resistance for Na/Na- $\beta'i$ – Al_2O_3 /Na cell. (e) Interfacial resistance as a function of heat treatment for Na/Na- $\beta'i$ – Al_2O_3 /Na symmetric cell. (f) Temperature vs. wetting angle for Na metal onto a $\beta'i$ – Al_2O_3 pellet with various surface treatment temperatures. (a), (b) Reprinted with permission from https://pubs.acs.org/doi/10.1021/acscentsci.6b00321. (a), (b) Reprinted with permission from [103] https://pubs.acs.org/doi/10.1021/acscentsci.6b00321. Copyright 2017 American Chemical Society. Further per-

missions related to the material excerpted should be directed to the ACS. (c)-(e) Reprinted with permission from Bay et al. [105]. Cop-yright 2020 Wiley. (f) Reproduced/Adapted from ref. [104] with permission from the Royal Society of Chemistry, Copyright 2018.104.



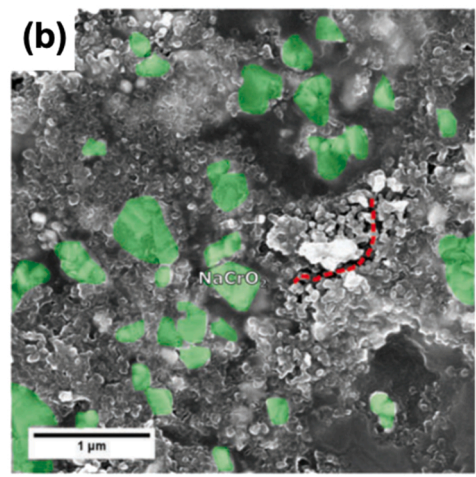


Fig. 6. Comparison of SEM micrographs for mixed cathode (a) and solution-processed cathode (b), showing micron sized cracking (red) for mixed cathode. (a) Reproduced/Adapted from ref. [108] with permission from the Royal Society of Chemistry, Copyright 2017.

2.2.3. Gel polymer electrolytes

The main limitation of SPEs is poor ionic conductivities at room temperature (generally $<10^{-4}\,\mathrm{S}\,\mathrm{cm}^{-1}$), which limits their practical utility. As a result, GPEs were developed as intermediates between commonly used liquid electrolytes and SPEs. [96] GPEs are processed by introducing a liquid plasticizer and/or solvent into a polymer-salt system. The transport of Na⁺ ions in GPEs is not dominated by polymer chain segmental motion, but rather occurs in the liquid phase regions of the swollen gel. [97].

The polymer membrane pore structures and the properties of trapped liquid electrolytes are key components in determining GPE ionic conductivities. [76,98] Some GPE properties required for practical applications include good mechanical strength, capacity to imbibe liquid electrolyte, high ionic conductivity, reasonable transference numbers and wide electrochemical stability. [76,99].

3. Methods for improving interfacial properties of NaSEs

Optimization of NaSE/electrode interfaces is crucial to fabricating safe and long-lasting NaSSBs (>1000 cycles). Interfacial interactions critically control cell cycle life and rate performance: chemical reactions at interfaces can degrade crystalline structures, increase impedance, and shorten cycle life. [100] In addition, unstable solid electrolyte interfaces (SEIs) that form as a result of continued, unwanted side reactions lead to capacity degradation. [101] Volume changes on intercalation of Na $^+$ can also occur, causing mechanical stresses leading to cracking and delamination. [93,102].

Reflecting on these issues, a desirable interface should: (1) allow fast ionic diffusion, but only with a stable SEI; (2) suppress dendrite growth and penetration into the NaSE; (3) be chemically and (4) mechanically compatible. Such properties require interfacial engineering methods, as detailed in the following sections. The primary focus of this section is oxide-type solid electrolytes, which are generally the most rigid and brittle and can therefore benefit the most from interfacial modifications. Moreover, formation of interfaces in NaSSBs with sulfide solid electrolytes is relatively easier due to their ability to be cold pressed onto the electrode.

3.1. Electrode wetting

Wetting is used to increase contact area between the electrode and electrolyte. The mechanism of increasing the contact area enables maximized ionic diffusion pathways to lower interfacial impedance. Such an increase in contact area also promotes even Na⁺ flux across the interface, which is further described below.

3.1.1. Anode wetting

One critical requirement of next-generation batteries is fast charging for high-energy- and high-power-density applications. The reversible stripping and plating of alkali metals at high current densities (> 10 mA cm⁻²) at ambient is a desirable target to enable fast charging. Studies show that critical current density (CCD)–the maximum endurable current density for a reversible NaSSB without failure–is correlated to interfacial resistance between the solid electrolyte and anode. [18].

Anode wetting involves uniformly coating molten Na ($T_m = 98$ °C) onto an electrolyte surface. If done properly, this can provide an even Na⁺ flux across the interface, thereby limiting dendrite formation and propagation. Different heat and surface treatments have been explored targeting uniform anode coatings [103,104] as shown in Fig. 5a-b.

Uniform wetting both prevents dendritic growth and lowers interfacial resistance. Zhou et al. [103] studied the effects of Na wetting conditions in Na/NASCION/Na symmetric cells, finding the resistance of properly wet cells to be an order of magnitude lower than those with poorly wet interfaces. Additionally, Bay et al. found that heat treating $\beta' I - \text{Al}_2\text{O}_3$ pellets prior to applying Na metal can lead to stable potential responses in CCD measurements as high as 5 mA cm⁻² (see Fig. 5c). [105] This is likely due to the elimination of surface hydroxyls and carbonates, decreasing impedance. Na/ $\beta' I - \text{Al}_2\text{O}_3$ /Na symmetric cells withstood high CCDs at room temperature, ≤ 10 mA cm⁻², enabled by reducing interfacial resistance from 20 k Ω cm² (no heat treatment) to 10Ω cm² (heating at 900 °C) in Fig. 5d-e. [105].

In addition to heat treatments, Chang et al. [104] demonstrated that chemical modification of the electrolyte surface can decrease the Na metal wetting angle. In this study, the surface of a $\beta'\prime$ – Al_2O_3 electrolyte was treated with lead acetate trihydrate (LAT) at various temperatures. It was found that treatment at 400 °C decreases the wetting angle compared to other samples tested, seen in Fig. 5f.

Microscopic examination of the surface of the LAT-400 °C reveals the presence of micron-sized spherical particles of lead on the $\beta'\prime-Al_2O_3$ electrolyte that were not present in any of the other formulations. These spherical particles roughen the $\beta'\prime-Al_2O_3$ surface, which may account for its increased wettability. [104] In short- and long-term cycling tests, LAT-400 °C coated surfaces maintain stable capacities (~150 mAh g $^{-1}$ for the first 10 cycles) and a high CE (100% \pm 0.05%) over the first 80 cycles. Unfortunately, lead is highly toxic, and seems unlikely to be useful for anode wetting on a large scale.

3.1.2. Cathode wetting

Analogous to LIBs, cathode/electrolyte interfaces in Na-based batteries can be a major source of performance degradation and eventual failure. It is well understood for LIBs that at high voltages, most problems are observed at the cathode interface. This relationship is also observed in NaBs. High voltage (HV) cathodes are preferred for higher energy densities. You et al. [106] summarized the deleterious effects of HV sodium cathodes as: (1) catastrophic volume changes arising from phase transitions; (2) oxidation of electrolyte, and (3) oxygen loss created by deep charging of Co-based materials.

The issues highlighted by You et al. [106] also apply to NaSSBs. The reactivity of alkali metals often causes researchers to focus on anode-solid electrolyte interactions in lieu of the cathode-interface. Asakura et al. [107] generated a passivation layer of Na₄(CB₁₁H₁₂)₂(B₁₂H₁₂) formed in situ at 4.2 V by decomposition of Na₄(CB₁₁H₁₂)₂(B₁₂H₁₂) as (B₁₂H₁₂)₂ on the surface of the high voltage sodium cathode, Na₃(VOPO₄)₂F⁻. Above 4.2 V, electrolyte decomposition forms (CB₁₁H₁₂)⁻, which acts as a blocking interphase. This interphase passivates the cathode surface against further reactions. The hydroborate electrolyte can be introduced into the cathode as a catholyte via solution processing. [107].

3.2. Solution processing

Volume changes and chemical reactivity inherent with electrochemical cycling often lead to delamination of the solid electrolyte from the electrode, increasing interfacial impedance and decreasing cycle life. In addition to choosing electrode/electrolyte combinations with low reactivity, methods that lead to more intimate interfacial contact can also prevent delamination. [58,102,108] Solution processing involves dispersing a ceramic electrolyte with electrode material in a carrier liquid and subsequent drying, which results in a catholyte with uniform electrolyte coating and high surface coverage. [58,109] The improved contact between solid electrolyte and active material results in enhanced ionic conductivity and charge transfer at the interface. Fig. 6 provides an example of how this method leads to superior mechanical contact within the catholyte. In this study, Duchêne et al. [108] compared the performance of two catholytes: one made by simply ball milling electrolyte particles $[\mathrm{Na_2}(\mathrm{B_{12}H_{12}})_{0.5}(\mathrm{B_{10}H_{10}})_{0.5}],$ carbon black, and active material (NaCrO₂), and another by the solution processing method described above.

In the latter approach, the first step is to dissolve the sodium closoborate electrolyte and formulate a dispersion with $NaCrO_2$ active material in anhydrous methanol. The catholyte is then vacuum dried and subsequently ground with more electrolyte and conductive carbon. The end mass ratio of active material (AM), solid electrolyte (SE), and conductive carbon (CC) was the same as the ball-milled catholyte (70:20:10 AM:SE:CC).

Catholyte cells of the form catholyte/closo-borate/Na were then tested. On cycling at 6 mA g $^{-1}$ (C/20), the ball-milled catholyte presented a low first cycle CE, which increased to above 90% by the third cycle, resulting in excessive capacity loss due to poor contact between solid electrolyte particles and active material. The solution-processed catholyte showed a much higher first cycle CE of 89%, which increased to > 99% on further cycling. The cell with the solution-processed catholyte retained 94.6% of the initial discharge capacity after 20 cycles at C/20. This 3 V cell was cycled at rates up to 24 mA g $^{-1}$ (C/5), showing minimal capacity loss after 250 cycles. Note that while these current rates are slightly lower than what is required for most applications, the comparison between the ball-milled and solution-processed catholytes shows significant promise for the latter.

In EIS measurements, the impedance of the solution-processed catholyte was roughly an order of magnitude lower than the ball-milled catholyte. [108] This result implies that both the charge transfer and charge transport resistances within the bulk of the solution-processed catholyte were reduced due to the improved contact between the closo-borate and NaCrO₂ particles through active material impregnation. In a later work, Asakura et al. [107] used this same solution processing technique to achieve a stable NaSSB operating at 4 V.

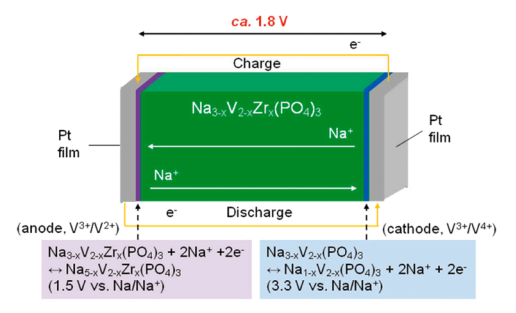


Fig. 7. Schematic of $Pt/Na_{3-x}V_{2-x}Zr_x(PO_4)_3/Pt$ cell with \approx zero-resistance interface

Reprinted with permission from Inoishi et al. [110]. Copyright 2016 Wiley

3.3. Zero-resistance interfaces

Often, compatibility optimization directly dictates the eventual utility of a battery system. In this vein, Inoishi et al. [110] explored the use of single phase materials with inherent compatibility centered around $Na_{3-x}V_{2-x}Zr_x(PO_4)_3$ (NVZP) from the NASICON family. The composition was varied between cathode, electrolyte, and anode resulting in virtually resistance-free interfaces. Using a single phase for all three primary cell materials, high temperature sintering can be used without formation of damaging interface reaction layers. After initially charging (Fig. 7), only electrolyte resistance was observed.

Inoishi et al. [110] showed that despite higher electrolyte resistance, the all-NVZP cell offered lower overall cell resistance compared to other NASICON-type cells. This is attributed to the absence of interfacial resistance (50 vs. 20 k Ω). In a cell using electrodes with conductive additive (Na_{3-x}V_{2-x}Zr_x(PO₄)₃ with vapor grown carbon nanofibers) ~55% of theoretical capacity (64 mAh g⁻¹) was achieved. [110].

In this study, the authors demonstrate the possibility of using a single material with optimized compositions to fabricate a full cell, which eliminates the need for additional interfacial modification and reduces cost. However, this strategy is still in the early stages of development. More materials should be explored to improve electrochemical performance. Achieving an appreciable voltage difference from electrodes made of the same material may also pose a challenge to this technology.

3.4. Co-sintering

While still in the developing stages, co-sintering the cathode and inorganic solid electrolyte is one approach to improving mechanical stability and interfacial contact. For instance, Zhang et al. [50] sintered a NASICON electrolyte pellet coated with Na₃V₂(PO₄)₃ (NVP) active material and achieved a CE of nearly 100% at 10 C/10,000 cycles/25 °C. In this study, however, such results required adding a drop of ionic liquid (IL) to the cathode side after sintering the materials separately. The benefits of IL in improving charge transfer at the interface are discussed further in Section 4.2. When cycled at 0.1 C/80 °C, the all-solid-state co-sintered cell without ionic liquid experienced significant capacity fading within the first 40 cycles. [50].

While co-sintering is beneficial for enhancing interfacial stability, it has several disadvantages when used in NaSSBs. For example, Lalère et al. [111] consolidated an NaSSB using spark plasma sintering, but this cell required an operating temperature of 200 °C to achieve reasonable ionic conductivity. Another report of co-sintering a layered cathode with $\beta'\prime-{\rm Al_2O_3}$ also required elevated operating temperatures (350 °C) to reduce polarization. [112] There are several reasons that co-sintering leads to high interfacial impedance: this method has been found to produce side reactions [113–115] and high elemental interdiffusion rates, [116] both of which can lead to formation of unwanted interphases that impede ionic transfer.

The thicknesses of these interphases can grow with continued Na⁺

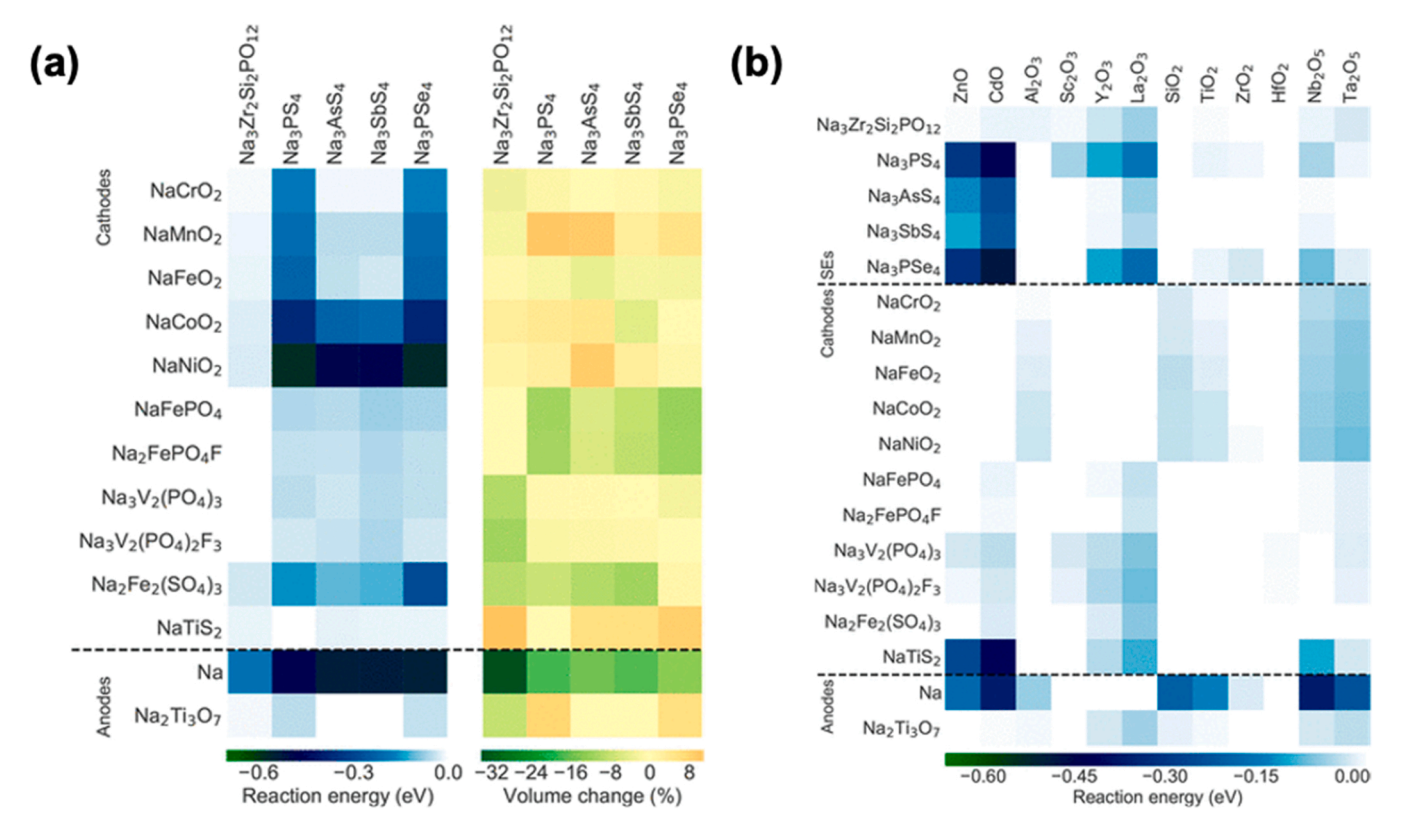


Fig. 8. Interfacial reactivity and volume changes for common electrode/electrolyte pairs (a) and reaction energy of buffer layers with electrolytes, cathodes, and anodes.

(b). Reprinted (adapted) with permission from Tang et al. [93]. Copyright 2018 American Chemical Society.

extraction/insertion, deteriorating capacity and lowering CE during cycling. Attempts to construct NaSSBs based on co-sintered mixed electrodes find severe capacity degradation in the first few cycles. [110, 117] While co-sintering does have several drawbacks, its utility in fabricating all-solid-state batteries cannot be ignored, and more studies will be critical in understanding the connection between interfacial properties and impedance.

4. Interfacial additives: buffer layers, ionic liquids, polymer electrolytes

In addition to controlling interfacial stability via engineering solutions, the addition of materials to the interface can also improve stability and cycle life. Examples include buffer layers (BLs), ILs, and polymer electrolytes. The way these materials aid interfacial stability is discussed below.

4.1. Buffer layers

Different crystal structures and chemical potentials between interfacial materials can lead to reactivity that degrades active material and battery performance. [93] Also, volume changes due to Na^+ (de)intercalation on cycling can cause mechanical defects including cracking and delamination that further remove active material from the cell. BLs are materials placed between the electrode and electrolyte that are intended to mitigate interfacial reactions and volume changes associated with cycling. BLs provide a stable, physical barrier that limits interfacial reactivity.

A good BL should have limited reactivity with both the electrode and electrolyte, reasonable diffusion rate of the mobile cation, and nanometer thickness. Also, a BL is not beneficial when used at an otherwise stable interface, as it is a barrier to ionic diffusion.

To determine which BLs to use, it is first necessary to examine the interfacial reactivity and volume changes that occur on cycling for common electrode/electrolyte pairs. Tang et al. [93] used density functional theory calculations to simulate reactivity between electrolytes and several cathodes/anodes (Fig. 8). Note that full thermodynamic equilibria were assumed.

From Fig. 8a, it is evident that layered NaMO $_2$ (M=Cr, Mn, Fe, Co, Ni) cathodes are unstable with Na $_3$ PS $_4$ or Na $_3$ PSe $_4$, likely due to displacement reactions that form phosphate compounds. Also, Na $_3$ Zr $_2$ Si $_2$ PO $_{12}$ (NZSP) shows low volume change on Na $^+$ (de)intercalation with all oxide cathodes, suggesting that an oxide cathode/NZSP cell would have good mechanical stability. On the anode side, pure Na metal shows poor chemical and volumetric stability against all solid electrolytes. The Na $_2$ Ti $_3$ O $_7$ anode, however, has much lower volume expansion with the electrolytes tested. This demonstrates the enhanced stability of a Nacontaining compound as an anode (see Na $_2$ Sn in Table 4 for another example). Nonmetal anodes are also beneficial for fabrication because most do not require an inert environment, reducing the cost for assembly of NaSSBs.

While thermodynamic reaction energy provides a good starting point for probing electrode/electrolyte compatibility, it is not sufficient for determining stable cell chemistries: other factors that are key for cell stability–such as electrode passivation–were not considered in Fig. 8. Therefore, the discussion here is somewhat limited. Nevertheless, it is still useful to examine the deleterious effects of volumetric expansion between the electrode and electrolyte that can accelerate delamination and other mechanical issues in an NaSSB.

Tang et al. [93] also analyzed the reaction energy of common oxide BLs with solid electrolytes, cathodes, and anodes (see Fig. 8b). Al₂O₃, a common BL, shows low reactivity with solid electrolytes and cathodes and only slight reactivity with Na metal, making it a suitable BL for most interfaces. Of all BLs studied, only HfO₂, Sc₂O₃, and ZrO₂ present high

Table 4Symmetric Cell Performance for Sodium-Ion Electrolytes with Anode Materials.

Cell (electrode = Na if unlisted, electrolyte)	Current Density (mA cm ⁻²)	Voltage Window (V)	Other Considerations	Ref.
PVDF-NaCF ₃ SO ₃ -SiO ₂	• 0.2	0 – 4.1	• 25°C	[127]
			 5 μL cm⁻² of liquid electrolyte added to both electrodes 	
			• Cycled stably > 1000 h	
$Na-\beta' \prime - Al_2O_3$	• 10		• 25 ℃	[105]
			Critical current density	[103]
NZSP	 0.8 (stable at 25°C) 		 Gradual voltage increase in galvanostatic cycling at 0.9 mA cm⁻², 25°C 	[128]
	 3.0 (stable at 90°C) 		Cells pressed at 30 MPa	
Na ₂ Sn, Na ₃ PSe ₄	• (stable)	1.25 - 2.35	• 25°C	[126]
	• 0.2 (unstable)		 Symmetric cell with Na₃PSe₄ and Na anodes experienced increasing polarization during cycling at 0.1 mA cm⁻² 	
Na ₂ Sn, Na ₃ PS ₄	• 0.2	0.9 - 2.5	• 25°C	
			 Stable cycling at 0.1 mA cm⁻²/50 h, 0.2 mA cm⁻²/70 h 	
NZSP	• 0.25	0 - 5	• 65°C	[103]
			Stable cycling to 475 h	
			 NZSP wet with Na at 380°C 	
			 Cells without wetting fail in 1 h under 0.15 mA cm⁻² 	
CPMEA-NZSP-CPMEA	• 0.2		• 65°C	
			Stable cycling to 380 h	
$Na_{3.4}Zr_2Si_{2.4}P_{0.6}O_{12}$	• 0.6		• 25°C	[129]
			Cycled stably for 300 h	
$Na-SiO_2$, $Na_{3.2}Zr_{1.90}Mg_{0.10}Si_2PO_{12}$	 0.2 (stable for 130 h) 		• 25°C	[130]
	 0.5 (critical current density) 		\bullet Cell with Na anodes prepared by pressing failed at 0.1 mA cm $^{-2}$ $<$ 10 h	
Na _{3.1} Zr _{1.95} Mg _{0.05} Si ₂ PO ₁₂	• 0.044	0 – 4.5	• 25°C	[47]
			• Stable polarization potential of 2.7 mV obtained cycling test for over 50 h	
Na ₂ (B ₁₂ H ₁₂) _{0.5} (B ₁₀ H ₁₀) _{0.5}	• 0.1	0 - 3	• 60°C	[131]
			Stable cycling for 12 days	
Na _{1.67} Al _{10.33} Mg _{0.67} O ₁₇	• 0.044	_	• 25°C	[41]
			Stable cycling for 6000 s	
			 Electrolyte doped with TiO₂ and ZrO₂ 	
NZSP-NaClO ₄ -PEO	• 1.0		• 60°C	[91]
			Stable cycling for 500 h	
PVDF-HFP coated	• 0.5	0 - 4.8	• 25°C	[00]
Na– $\beta' \prime$ – Al ₂ O ₃ nanowires			 Stable polarization potential for 300 h 	[92]
			 Stable cycling for 100 h at 2 mA cm⁻² 	

 $\begin{aligned} \textbf{NZSP} &= Na_3Zr_2Si_2PO_{12} \ | \ \textbf{CPMEA} = \textbf{cross-linked poly(ethylene glycol) methyl ether acrylate} \ | \ \textbf{PVDF-HFP} = \textbf{poly (vinylidene fluoride-co-hexafluoropropylene)} \ | \ \textbf{PVDF} = \textbf{polyvinylidene fluoride} \end{aligned}$

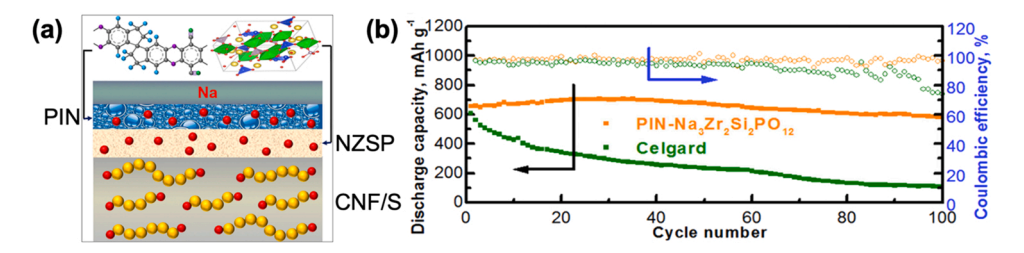


Fig. 9. Schematic of NASICON-type NaSE coated with a novel polymer with intrinsic porosity (PIN) to enhance interfacial contact (a) and long-term cycling at C/5 showing improvement using PIN-NZSP over traditional Celgard..

(b). Reprinted from Yu and Manthiram [119]. Copyright 2019, with permission from Elsevier.

stability with both the Na anode and sulfide/selenide SEs. Lastly, ${\rm SiO_2}$ offers good stability vs. solid electrolytes and polyanionic cathodes, making it an inexpensive and ideal BL for this interface.

 HfO_2 has been coated onto MoS_2 anodes via atomic layer deposition to produce a nanometer thick BL, which allows for facile Na^+ diffusion due to the amorphous nature of HfO_2 . [118] When the MoS_2 was cycled with and without a BL, the HfO_2 -coated anode delivered 99.6% CE over the first 50 cycles while the bare anode delivered only 98.6% CE, resulting in noticeable capacity fading. While not technically classified as a rare-earth metal, Hf is expensive, which could be a barrier to commercialization.

Polymer coatings can also make suitable buffer layers. Yu et al. [119] leveraged the high ionic conductivity and polysulfide-blocking nature of NASICON-type NZSP with a nanoporous polymer (PIN) buffer layer to enhance interfacial properties. The intrinsic nanoporosity allows for

facile ion diffusion while maintaining a flexible "cushion" between the ceramic and Na metal. This reduces the probability of fracturing the ceramic separator when applying enough pressure to create an ideal interface. In this study, carbon nanofibers (CNFs) were added on the cathode side to improve the electronic conductivity.

A CNF/S||NZSP-PIN||Na full cell was constructed and outperformed a similar cell using only a Celgard separator in liquid electrolyte. High capacity retention (550 mAh $g_{\rm sulfur}^{-1}$ after 50 cycles @ C/5) is realized for the NZSP-PIN system compared to immediate capacity degradation in the Celgard-based cell, shown in Fig. 9 below. [119].

4.2. Ionic liquids

Adding ILs to electrode/electrolyte interfaces has been shown to increase solid particle contact and charge transfer rates, mitigate volume

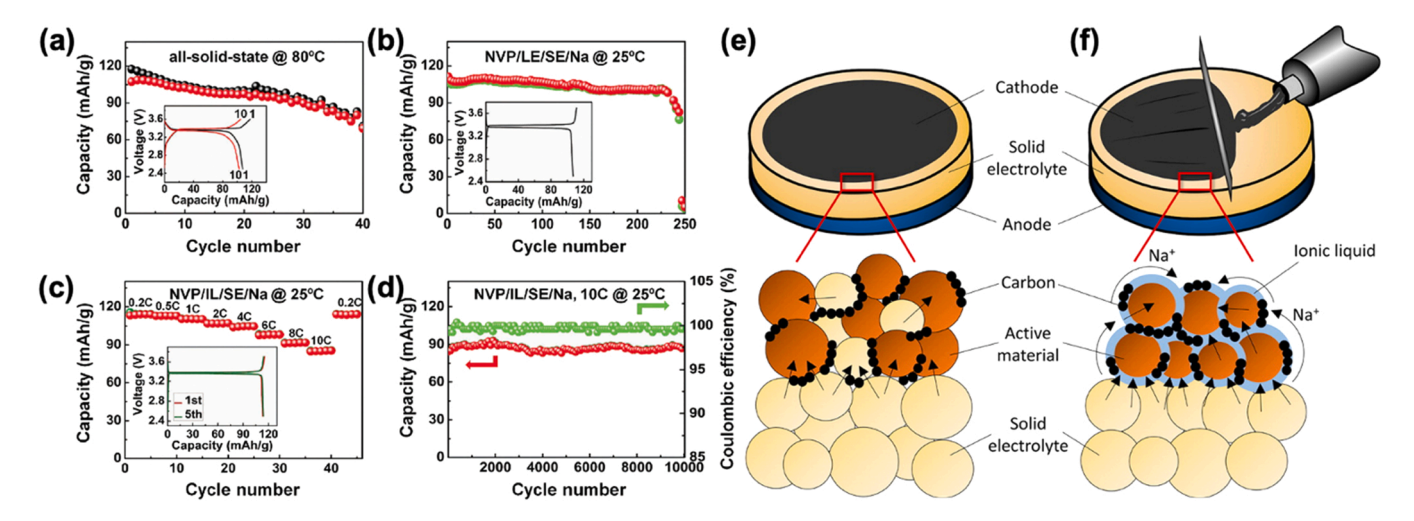


Fig. 10. The electrochemical performance of solid-state batteries. (a) NVP/SE/Na NaSSB operating at 80 °C (b) NVP/LE/SE/Na hybrid battery operated at 0.2 C at ambient. (c) Rate performance of the NVP/IL/SE/Na solid-state battery at various current densities at ambient. (d) Cycling performance and coulombic efficiency of the NVP/IL/SE/Na solid-state battery at room temperature with a current rate of 10 C for 10000 cycles. (e) Schematic of cathode/solid electrolyte interface without ionic liquid and (f) with ionic liquid. (a)-(d) Reprinted (adapted) with permission from Zhang et al., *Adv. Energy Mater.*, 2017, 7 (4), 1601196. [50] Copyright 2017 American Chemical Society. (e), (f) Reprinted (adapted) with permission from Liu et al., *ACS Appl. Mater. Interfaces*, 8 (48), 32631–32636 (2016). [120] Copyright 2016 Wiley.

changes associated with cycling through hydrostatic stress dispersion, and enhance mechanical stability. [50,120] Also, ILs are non-flammable and non-volatile, making them practical for use in NaBs.

In a study by Zhang et al., [50] the cycling performance of three different cells was compared. All three cells were of the general form NVP/SE/Na; the SE was from the NASICON family. In addition to this, cells were made by adding (a) 5 μL cm 2 of organic liquid electrolyte (0.8 M NaPF $_6$ salt in ethylene carbonate-dimethyl carbonate, LE) and (b) 5 μL cm 2 of ionic liquid (N-methyl-N-propylpiperidinium-bis (fluorosulfonyl) imide) as interfacial wetting agents on the cathode side. The cycling results for all three cells are shown in Fig. 10.

As seen in Fig. 10a, the co-sintered NVP/SE/Na cell showed

significant capacity fading and low CE over the first 40 cycles, as discussed in Section 3.4. The cell with liquid electrolyte showed good capacity retention for about 225 cycles, then quick capacity fading and ultimate failure by 250 cycles (Fig. 10b). Finally, in Fig. 10d, the cell with IL showed a first cycle CE of 97.5% and an average CE of $\sim\!100\%$ over 10,000 cycles at 10 C, maintaining a capacity of 90 mAh g $^{-1}$ (the discharge capacity at 0.2 C was 113 mAh g $^{-1}$ in Fig. 10c). The ionic liquid aided cycling performance by enhancing solid particle contact between interfacial materials, providing a new ion migration channel to lower impedance, and allowing a buffer space for volume expansion in the cathode during electrochemical cycling. [50,121].

Liu et al. [120] mixed a layered $Na_{0.66}Ni_{0.33}Mn_{0.67}O_2$ with IL and

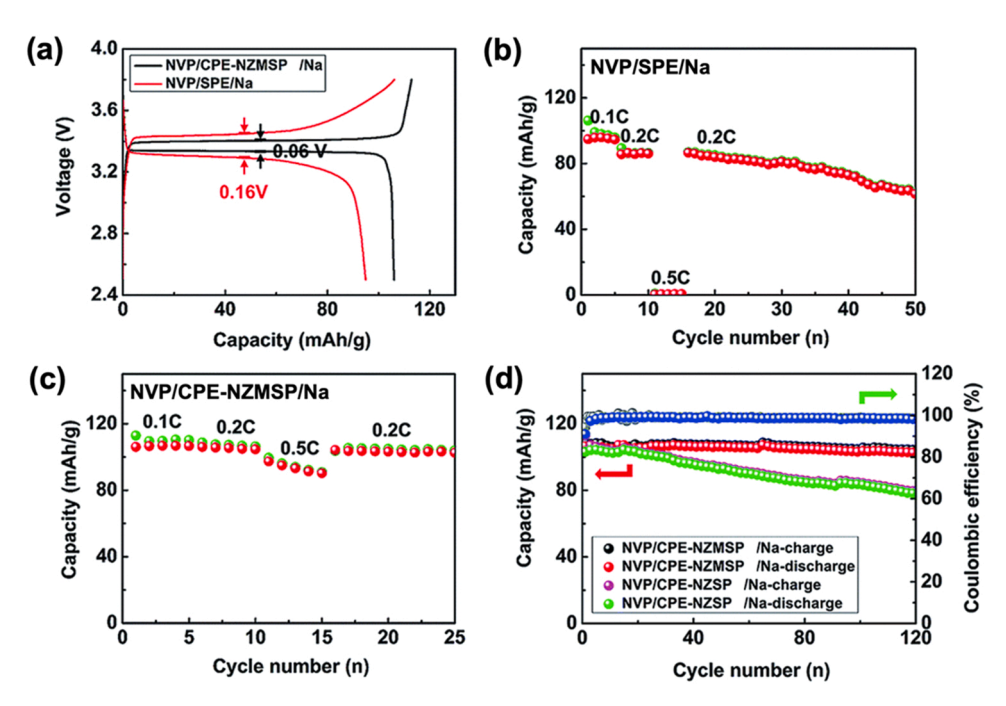


Fig. 11. (a) The 1st charge/discharge curves of the NVP/CPE-NZMSP/Na and NVP/SPE/Na batteries at 0.1 C and 0.2 C; (b) the rate performance of the NVP/SPE/Na batteries at various C-rates; (c) the rate performance of the NVP/CPE-NZMSP/Na batteries at 0.1 C, 0.2 C and 0.5 C; (d) the cycling performance of the NVP/CPE-NZMSP/Na cells at 0.2 C under 80 °C.

(d) Reprinted from Zhang et al. [75]. Copyright 2017, with permission from Elsevier. [75].

applied this soft electrode onto a $\beta'\prime$ – Al_2O_3 solid electrolyte pellet (see schematic in Fig. 10e-f). The IL acts as mobile cation conductor, wetting agent, and binder to increase solid interparticle contact. Solid-state batteries synthesized with this solution processed electrode showed excellent stability, maintaining a CE near 100% after 10,000 cycles at 6 C. The capacity retention after 10,000 cycles was 90%, and a capacity of 79 mAh g⁻¹ was recovered when the current rate was returned to 0.1 C. It should be noted that this study was performed at 70 °C, where the conductivity of $\beta'\prime$ – Al_2O_3 (\sim 1 ×10⁻² S cm⁻¹) is nearly an order of magnitude higher compared with ambient (\sim 1 ×10⁻³ S cm⁻¹). [122, 123] The addition of ionic liquid also led to remarkable stability at high current rates.

4.3. Polymer electrolytes

Due to their flexibility and ionic conductivity, composite polymer electrolytes are reported to improve cycling performance by achieving intimate contact with both the ceramic filler and electrode material. [124] The polymer electrolyte in general enhances stability by suppressing dendritic growth. [92] It also allows for effective interfacial contact and good chemical compatibility with common electrodes. [125] Furthermore, the rate performance of CPEs is superior to that of solid polymer electrolytes due to the additional ion migration channels provided by the ceramic electrolyte.

It has been shown through cycling tests that cells made with CPEs can achieve higher electrochemical stability, better rate performance, and lower polarization than those with SPEs. [75,91,92,95] An example is shown below in Fig. 11. In this study, the electrochemical performance of a NaTFSI/PEO-based SPE was compared with that of a Na $_{3.4}$ Zr $_{1.8}$ Mg $_{0.2}$ Si $_{2}$ PO $_{12}$ (NZMSP)-based CPE.

In Fig. 11b, the rate performance of the half-cell with SPE is poor; it experiences fading capacity at 0.2 C, and the capacity delivered at 0.5 C is less than half that at 0.1 C. The half-cell with CPE-NZMSP in Fig. 11c shows only a minimal capacity dip at 0.5 C. This study also included the longer-term cycling performance of the CPE-NZMSP, which maintained $\sim\!100\%$ CE for the 80 cycles tested (see Fig. 11d).

Filler conductivity also influences electrochemical performance. In a previous study by Zhang et al., [95] the long-term cycling performance of a cell with CPE-NZMSP was compared to an identical cell with NZSP as CPE filler. Due to the superior ionic conductivity of NZMSP (at ambient, 1.6 mS cm⁻¹ for NZMSP and 0.67 mS cm⁻¹ for NZSP), the cell with CPE-NZMSP achieved a CE of nearly 100% over 120 cycles at 0.1 C while the CPE-NZSP cell experiences notable capacity fading under the same conditions.

4.4. NaSE performance in symmetric cells

In this section, a summary of NaSE rate performance is given in the context of symmetric cells. Symmetric cells can be used in galvanostatic cycling experiments to measure the cycling stability of an electrode/ electrolyte pair at a given current density. Na metal is the most common electrode in symmetric cells. However, as outlined in Section 4.1, Na reacts strongly with most electrolytes, degrading crystalline structures at anode/electrolyte interfaces. [93].

As with LIBs, other anodes including Na_2Sn or $Na_2Ti_3O_7$ offer increased stability. [126] Symmetric cell data for various anode/electrolyte pairs is summarized in Table 4. Note that several of the examples in Table 4 use an interfacial modification method from Sections 3 and 4 to enable better cycling capabilities and rate performance. [103,127, 128].

Per Table 4, many different symmetric cell formulations offer good stability at ambient and at high current densities (>1 mA cm 2). [91, 105,128] The Na/NASICON interface shows high stability at various temperatures and cycling conditions. [47,103,129] The voltage window up to $\sim\!4.5$ V vs. Na makes this interface ideal for use in high-energy half/full-cells with an appropriate cathode. Use of a high conductivity

Table 5Symmetric Cell Performance of Sodium-Ion Electrolytes with Cathode Materials.

•			•	
Cell (electrode, electrolyte)	Current density (mA cm ⁻²)	Voltage window (V)	Other considerations	Ref.
NVP, NZSP	• 0.097	0 – 2.2 (avg. of 1.8)	• 200°C • Electrode: 25% NVP / 60% NZSP / 15% Carbon • 60% initial capacity retention at 0.486 mA cm ⁻²	[111]
NVP, PVDF- NaCF ₃ SO ₃ -SiO ₂	• 0.5 C	1 – 2.5 (avg. of 1.7)	 25°C Capacity fading for first 50 cycles 70% capacity retention after 100 cycles 5 μL cm⁻² of liquid electrolyte added to both electrodes 	[127]
NMTO, NZSP- PEO (25 wt% PEO)	• 0.01		 25°C Stable cycling for 100 cycles with polarization of 0.2 V 	[132]

 $\begin{array}{l} \textbf{NVP} = \mathrm{Na_3V_2(PO_4)_3} \mid \textbf{NZSP} = \mathrm{Na_3Zr_2Si_2PO_{12}} \mid \textbf{NMTO} = \mathrm{Na_{0.44}Mn_{0.67}Ti_{0.33}O_2} \mid \textbf{PEO} = \mathrm{polyethylene} \ \mathrm{oxide} \mid \textbf{PVDF} = \mathrm{polyvinylidene} \ \mathrm{fluoride} \end{array}$

electrolyte such as $Na_{3,4}Zr_2Si_{2,4}P_{0,6}O_{12}$ (4.8 mS cm⁻¹ at ambient [129]) is also shown to decrease electro-polarization by reducing cell impedance. [47,129] While Na metal is a preferable anode due to its high theoretical specific capacity, it is incompatible with Na_3PX_4 (X = S, Se) electrolytes. Substitution of pure Na with Na_2Sn offers more stable cycling performance. [126].

Cathode materials such as NVP have also been used in symmetric cells to study compatibility with electrolytes. [111,127] Table 5 summarizes the data on symmetric cells with cathodes. In general, regardless of electrode material, symmetric cells with engineered controls including anode wetting (see Section 3.1.1) [103] and solution processing of the electrolyte (see Section 3.2) [108] perform favorably in galvanostatic cycling experiments.

5. Cathodes enabling high-energy NaSSBs: design and implications

One critical element for high-energy-density NaSSBs is optimizing cathode materials. There is good agreement between NaBs, LIBs, and NaSSBs, in that the respective alkali metal anode provides the most promise for high energy density and capacity. As emphasized in Sections 3 and 4, the Na metal interface with SEs is challenging to optimize and is often limited to non-reactive material pairs that do not decompose or form side products on contact or cycling. Efforts have been made to passivate both cathode and anode interfaces with SEs in NaSSBs with moderate success. [50,103,104,107,108] If Na metal is assumed to be the anode of choice, the cathode is the next variable in efforts to increase cell energy density. Cathodes such as NVP and NMTO have been explored in symmetric cells using NaSEs. [111,127,132,133].

SOTA cathodes for NaSSBs must balance high capacity, operating voltage, and stability. Generally, NaBs have lower operating voltages compared to LIBs due to differences in electropositivity. For this reason, novel sodium cathode studies focus on specific capacity instead of energy density – especially when comparing to LIBs. The primary comparison for SOTA energy density is between oxide- and sulfur-based cathodes. Oxide-based cathodes favor higher operating potential, but lower specific capacity when compared to sulfur-based cathodes. Sulfur-based cathodes can have energy densities greater than 1400 Wh kg⁻¹, while oxide systems such as NVP typically have energy densities less than 600 Wh kg⁻¹. [134,135] In addition to high energy density, the low

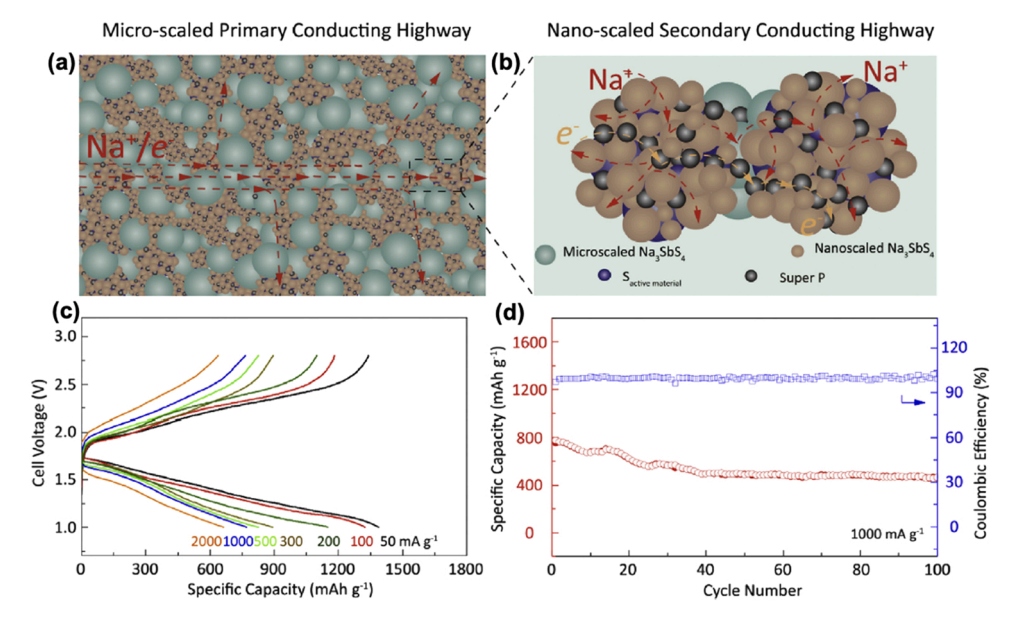


Fig. 12. Primary and secondary conducting pathways illustrated for Na₃SbS₄ NaSE shown in (a) micro-scale and (b) nano-scale, and performance data of specific capacity vs. voltage for varying (c) C-rates and (d) galvanostatic cycling up to 100 cycles at 1000 mA g⁻¹.

(a) Reprinted from Wan et al. [142]. Copyright 2020, with permission from Elsevier.

operating voltage of sulfur-based systems allows for high-voltage-incompatible materials to be utilized as NaSEs, such as polymers.

5.1. Sulfur-based cathodes

In general, the most desirable cathode is sodium sulfide, Na_2S . While Li-S batteries are also under development, Na-S batteries have been used commercially for decades with the caveat of an operating temperature above 300°C. [136] While this temperature is economically viable at

utility scales, it is unacceptable at the consumer level. In the previous decade, there has been significant progress towards ambient temperature Na-S batteries that offer high energy density (1274 Wh kg $^{-1}$). [134, 137,138] This improvement over the high temperature Na-S batteries arises from the different final discharge product (Na₂S vs. Na polysulfide). The different charge/discharge products are highlighted in Eq. (1) (high temperature) and 2 (room temperature) for Na-S cathodes. [134,136].

$$2Na + nS \quad \longleftrightarrow Na_2S_n \quad (n \ge 3) \tag{1}$$

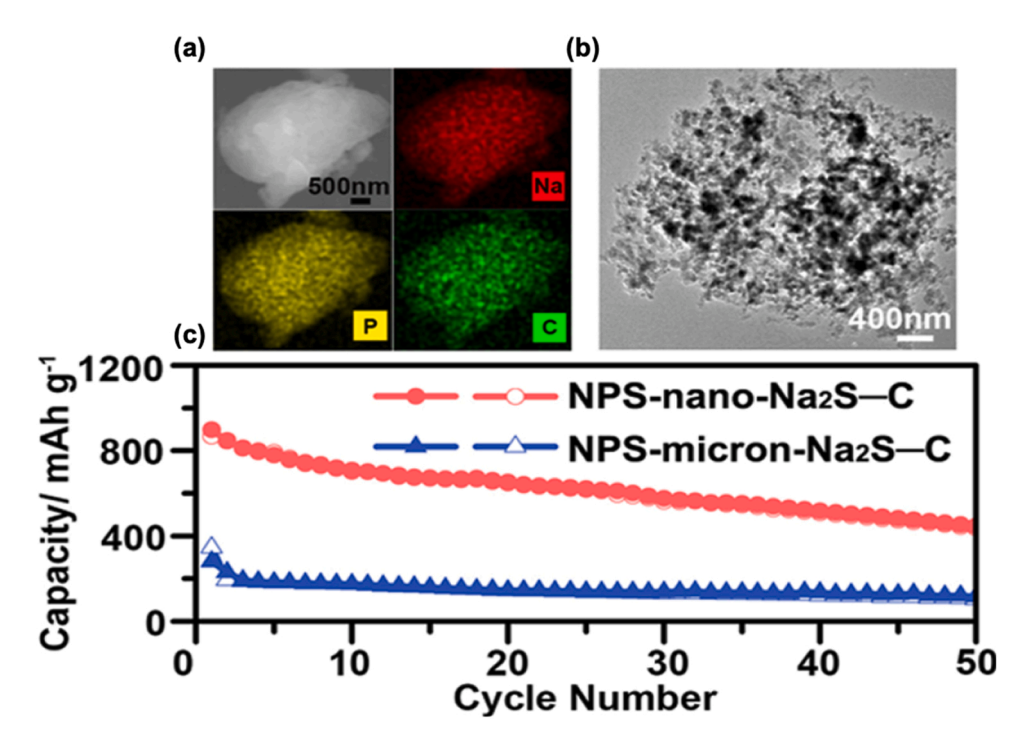


Fig. 13. Na₃PS₄ catholyte with nano- or micro-Na₂S-C, homogeneous elemental distribution shown by EDX (a), TEM image of composite cathode (b), and galvanostatic cycling.

(c)Reprinted (adapted) with permission from Yue et al. [141]. Copyright 2017 American Chemical Society.

Table 6
NaSSBs with a sulfur-based cathode and oxide-based electrolyte.

Cell (cathode, electrolyte, anode)	Reversible capacity, current density (mAh g ⁻¹ , mA g ⁻¹ or C-rate)	Interface Consideration	Ref.
S+C+PEO+NaClO ₄ +SiO ₂ + EMIM TFSI, NZMSP, Na metal	• 150	Polymer catholyte mixed with S active material in 1:1 mass ratio and uniformly coated onto NZMSP ceramic pellet and vacuum dried.	[47]
3Ni-NaCl, β'' -Al ₂ O ₃ , NiCl2		 83.1% capacity retention 	[140]
3Ni-NaCl, NASICON, NiCl ₂		 87.8% capacity retention 	[140]
S/C, β' -Al $_2$ O $_3$, Na metal	• 600 @ 1/ 64 C after 90 cycles.	 1 M solution of NaCF₃SO₃ in TEGDME applied to each electrode 	[137]

 $\begin{array}{lll} \textbf{EMIM TFSI} = 1\text{-}Ethyl\text{-}3\text{-}methylimidazolium bis(fluorosulfonyl)imide} \mid \textbf{NZMSP} \\ = Na_{3.1}Zr_{1.95}Mg_{0.06}Si_2PO_{12} & | \textbf{NMTO} & = Na_{0.44}Mn_{0.67}Ti_{0.33}O_2 & | \textbf{PEO} \\ = \text{polyethylene oxide} \mid \textbf{NASICON} & = Na_{1+x}Zr_2Si_xP_{3-x}O_{12} \mid \textbf{TEGDME} & = \text{CH}_3O \\ (\text{CH}_2\text{CH}_2\text{O})_4\text{CH}_3 & & \text{CH}_2\text{CH}_2\text{O} \\ + \text{CH}_2\text{CH}_2\text{O} & & \text{CH}_2\text{CH}_2\text{CH}_2\text{O} \\ + \text{CH}_2$

$$2Na + pS \quad \longleftrightarrow Na_2S_p \quad (p \ge 1) \tag{2}$$

The benefit to using a sulfur-based cathode is high energy density paired with low cost and low toxicity. [136] The cost of sulfur is almost trivial compared to that of lithium, nickel, or cobalt. Sulfur prices have gone up recently but remain below \$150 ton^{-1} . [136] Sulfur-based Na cathodes have been used in combination with many different solid electrolytes. [47,139,140] Some of the most common electrolytes are also sulfur-based, such as Na₃PS₄ and Na₃SbS₄. [141–143].

Solid-state battery performance relies on triple-phase contact between the active material, electronic additives, and NaSE. Wan et al. [142] employed a nanoscale electronic and ionic network to ensure intimate triple-phase contact between a S-NaSbS₄-C composite cathode and NaSbS₄ NaSE.

Wan et al. [142] predicted the need for microscale ionic/electronic highways within the cathode supported by nanoscale bridges to ensure continuous triple-phase contact. A network was structured using S-NaSbS₄-C composite further mixed with Super P carbon and microscale NaSbS₄ as shown in Fig. 12a-b below. [142] This provides both primary and secondary conducting pathways within the composite cathode. SEM-EDS mapping was used to confirm the intimate contact between the active material, NaSE, and electronically conductive additive.

The resulting performance is shown above in Fig. 12c-d. At 50 mA g 1 , Wan et al. [142] obtained ≈ 1500 mAh g_{sulfur}^{-1} initial discharge capacity. Using a more realistic current density of 1000 mA g^{-1} , S-NaSbS4-C/NaSbS4/Na metal cells show good capacity retention at room temperature. Even at a cathode loading of 12.74 mg cm $^{-2}$, full cells showed reversible discharge capacity of ≈ 470 mAh g_{sulfur}^{-1} . This high loading performance is important in demonstrating the possibility of scaling the system to high-energy-density cells, which could be used in energy-intensive applications such as EVs. [142].

Yue et al. [141] explored using a nano Na_2S cathode material combined with Na_3PS_4 to ensure interfacial contact between the cathode and Na_3PS_4 NaSE. Due to processing the catholyte with C, high-ionic-conductivity Na_3PS_4 can act as active material and NaSE. [141] Both micron and nano Na_2S were tested in full cell formats. Fig. 13 shows that nano Na_2S offers lower interfacial resistance and greater discharge capacity retention through cycling. This superior performance, along with homogeneous mixing of nano Na_2S and Na_3PS_4 ,

Table 7NaSSBs with a sulfur-based cathode and sulfide-based electrolyte.

Cell (cathode, electrolyte, anode)	Reversible capacity, current density (mAh g ⁻¹ , mA g ⁻¹ or C-rate)	Interface Consideration	Ref.
Na ₂ S-C-Na ₃ PS ₄ , Na ₃ PS ₄ , Na metal	• 870 @ 50 mA g ⁻¹	Nano-Na ₂ S catholyte (Na ₃ PS ₄) containing cathode provides good interfacial contact between cathode and NaSE due to only 2- phase requirement for charge transfer reaction.	[141]
S-(MSP-20)- Na ₃ SbS ₄ , Na ₃ SbS ₄ , Na ₃ SbS ₄ - Na ₃ PS ₄	• 1560 per sulfur (330 per composite) @ 0.064 mA cm ⁻²	Carbon matrix allows for expansion and contraction of activated S, further improvement can be made with particle size optimization. 1560 mAh g ⁻¹ initial and 93% capacity retention after 50 cycles.	[143]
S, 75Na ₂ S- 25 P ₂ S ₅ , Na metal	Only cyclic voltammetry	and so eyeles.	[139]
S-Na ₃ SbS ₄ -C, Na ₃ SbS ₄ , Na metal	• 743 @ 100 mA g ⁻¹ and 6.34 mg cm ⁻² loading	Nanoscale secondary ionic/electronic network promoting triple contacts resulting in good interfacial contact and low stress/strain on cathode material.	[142]

MSP-20 = phenol resin-derived activated carbon

reduces the need for triple-phase contact required for charge transfer reactions down to two-phase contact. Yue et al. [141] displayed ≈ 870 mAh $g^{\text{-}1}$ at 50 mA $g^{\text{-}1}$ in their NaSSB, which represented the best performance to that date. A comparison of the performances of solid-state Na-S batteries with oxide and sulfide-type solid electrolytes can be found in Tables 6 and 7, respectively.

The flexibility of CPE-based systems gives rise to inherently intimate electrode/NaSE contact. [47] The mechanical and conduction properties of CPEs can be improved by addition of an inorganic phase as described above. Zhu et al. [144] used a PEO-type SPE with low TiO_2 content as an inactive filler and NaFSI as electrolyte salt, shown in Fig. 14a-b. Different amounts of TiO_2 filler were tested, with the optimal content being only 1%. The composite cathode S/CPAN [CPAN = carbonized poly(acrylonitrile)] also contained SPE without TiO_2 to facilitate interfacial contact. Using this system, Zhu et al. [144] achieved 251 mAh g⁻¹ (710 mAh g⁻¹_{sulfur}) after 100 cycles (Fig. 14c) and good rate capability (Fig. 14d). See Table 8 for a performance comparison of solid-state Na-S batteries with CPE.

5.2. Oxide, phosphate, and hexacyanoferrate cathodes

Other promising cathode groups for NaSSBs are transition metal oxides, phosphates, and hexacyanoferrates. [148] Transition metal oxides such as NMC xyz (LiNi $_x$ Mn $_y$ Co $_z$ O $_2$) and NCA (LiNi $_x$ Co $_y$ Al $_z$ O $_2$ where x + y + z = 1) are well characterized and have dominated the LIB industry. The analogous sodium iterations have lower capacities but remain interesting as their structures are well understood from the LIB landscape. Phosphates such as NVP have been studied extensively and show promise with high theoretical capacity (118 mAh g $^{-1}$), capacity retention (96% over 200 cycles), and high-rate capability in liquid-electrolyte-based cells. [148] NVP is often used as a baseline for Na-based cathodes while testing other components, such as NaSEs.

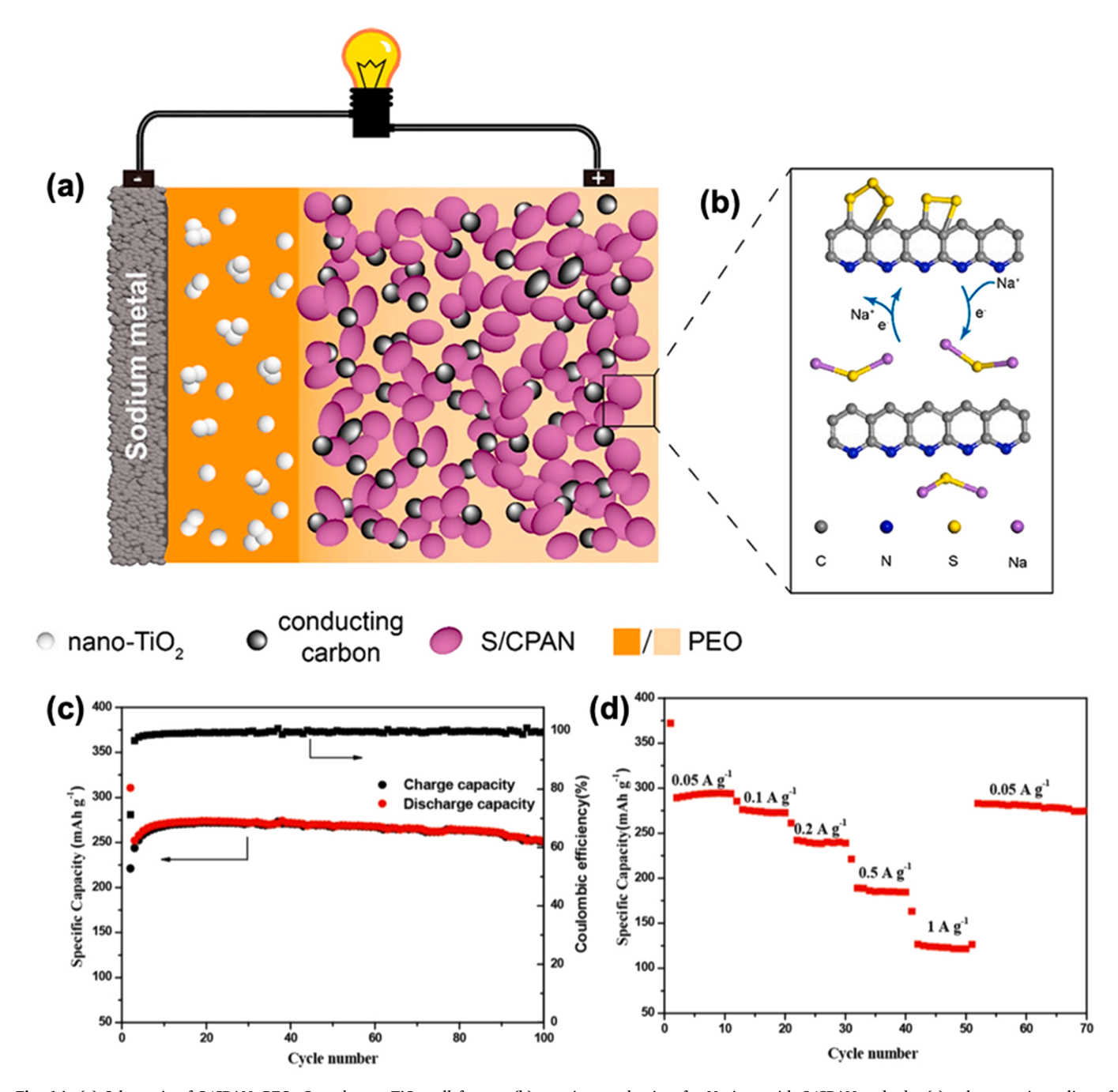


Fig. 14. (a) Schematic of S/CPAN, PEO, C, and nano-TiO₂ cell format, (b) reaction mechanism for Na ions with S/CPAN cathode, (c) galvanostatic cycling of assembled NaSSB, and (d) cycling test for assembled NaSSB at different rates. (d) Reprinted (adapted) with permission from Zhu et al. [144]. Copyright 2019 American Chemical Society.

Inherent issues such as low electronic conductivity can be overcome using different strategies including carbon coating, metal doping, and 3D porous architectures. [148–151] These strategies lead to high production cost, along with high material cost of V precursors. [148] Hexacyanoferrates have been of great interest in both academia and industry. A motivation for hexacyanoferrate and phosphate implementation is low cost per cathode energy – or \$/(Wh kg $^{-1}$) – and high energy density (Wh kg $^{-1}$) as shown in Fig. 15. [152].

Yu et al. [153] designed a laminated composite NaSE in conjunction with a low cost, high-energy-density hexacyanoferrate cathode. A PEO, succinonitrile (SN), NaClO $_4$ electrolyte was used at the anode interface due to its low voltage stability (< 4.2 V) and interfacial compatibility with Na metal (shown in Fig. 16b). On the opposite side, a PAN-based

CPE (PAN-NZSP-NaClO₄) was used to buffer the cathode interface. In both cases, the composite additives (SN and NZSP) were used to increase the Na $^+$ conductivity. Yu et al. [153] carefully matched the conductivities in both systems by tuning the PEO/PAN ratio with the respective Na $^+$ conductor. The result is a working NaSSB with a laminate-type NaSE, wherein neither layer individually can work independently of the other. The NaSSB cell had 83% capacity retention at C/5 over 200 cycles as shown in Fig. 16a. [153].

While most examples of NaSSBs do not show independent cathode/ anode interfacial tuning, certain chemistries can be compatible with both electrodes so individual tuning might not be necessary. Duchêne et al. [154] used closo-borate NaSE, Na₄(B₁₂H₁₂)(B₁₀H₁₀) (NBH) in solution form to impregnate a porous NaCrO₂ cathode, a concept

Table 8NaSSBs with a sulfur-based cathode and CPE.

Cell (cathode, electrolyte, anode)	Reversible capacity, current density (mAh g ⁻¹ , mA g ⁻¹ or C-rate)	Interface Consideration	Ref.
Poly(S-PETEA) @C, PETEA- THEICTA, Na metal	• 877 (736 after 100 cycles) @ 0.1 C	GPE successfully stabilized Na/NaSE interface while immobilizing soluble Na polysulfides. Poly (S-PETEA) strongly anchors S via chemical binding and reduces shuttle effect.	[145]
S/CPAN-PEO- NaFSI, PEO- NaFSI-nano TiO ₂ , Na metal	• 311 initial, 252 after 100 cycles, 0.1 A g ⁻¹	• S bonding to backbone of CPAN is key for reversible S cathode. Interface between composite cathode and NaSE has low resistance, 27.31 Ω.	[144]
PANI@C/S-280, PEO- NaCF ₃ SO ₃ - MIL-53(Al), Na metal	• 897 (675 after 50 cycles) @ 0.1 C	 Introduction of MIL-53 (Al) lowers interfacial resistance, improves cycling performance, increases Na trans- ference number and ionic conductivity. 	[146]
SnS ₂ , Na ₃ PS ₄ - PEO-NaClO ₄ , Na metal	• 230 @ 20 mA g ⁻¹ after 40 cycles	The addition of Na ₃ PS ₄ to PEO matrix improves interfacial contact between NaSE and cathode while also increasing ionic conductivity.	[147]

 $\mid \textbf{NPS} = \text{polyaniline} \mid \textbf{PEO} = \text{polyethylene oxide}$

introduced in Section 3.2. This infiltration increases the interfacial contact area and reduces porosity, thus optimizing ionic diffusion pathways through the catholyte (see Fig. 17 below).

The impregnated NBH electrolyte reduces porosity in the cathode and therefore aids in densification after pressing. Duchêne et al. [154] varied the pressing conditions and stack pressure to conclude that higher pressure results in better performance. The NBH-containing cell performed nearly identically to a cell with liquid electrolyte (118 vs. 121 mAh g⁻¹). See Table 9 for a performance comparison of more NaSSBs without a sulfur cathode.

6. Conclusions and future perspectives

This review summarizes current research on solid electrolytes and their interfacial stability with potential anode and cathode materials. In general, sodium-based oxide electrolytes exhibit high stability and offer many facile synthesis routes; however, their ionic conductivities are not as high as sulfide-based electrolytes. On the other hand, sulfide-based electrolytes have drawbacks such as poor thermal stabilities, brittleness, side reactions with electrodes (Na metal), and high moisture sensitivity. Numerous studies have targeted alleviating these shortcomings by introducing dopants and coatings to modify composition and structure. Furthermore, solid polymer electrolytes are also promising to enable NaSSBs with high flexibility and low-cost synthesis. In addition, dendrite growth may be suppressed in solvent-free polymer electrolytes under certain conditions.

Furthermore, we summarize current efforts to improve the interfacial and chemical stability of NaSSBs to achieve long-term cycling with minimal capacity loss. Significant improvements have been made using cathode solution processing, anode wetting, and CPEs to increase the contact area of interfacial materials. The introduction of buffer layers to the interface, such as alumina or ionic liquid, have also been shown to increase cycle life and rate capability. Ultrathin buffer layers accessible via chemical vapor deposition reduce interfacial impedance. In addition, computational studies have provided guidelines for selecting promising solid electrolytes and buffer layers that could enable the assembly of NaSSBs.

Moreover, these interfacial techniques have been used to improve the performance of sulfur, oxide-, hexacyanoferrate-, and phosphatetype cathodes in NaSSBs. Due to the high theoretical capacity of sulfur-based systems, most NaSSBs employ sulfur-based cathodes. While initial studies required high operating temperatures (>200°C) for adequate ionic conductivity, interfacial techniques discussed here permit reducing operating temperatures to near ambient while maintaining good performance. More well-known oxide-, hexacyanoferrate-, and phosphate-based cathodes such as NaCrO2, Na2MnFe(CN)6, and NVP are also possible candidates. In these cathodes, high capacity is sacrificed at the expense of cycling stability. Independent of cathode type, introduction of ionically-conductive pathways enables high areal loadings such that the cell format has a wider breadth of potential applications. The introduction of ionically-conductive agents is critical for reducing interfacial resistance while also maximizing contact between active material and electrolyte.

To produce next-generation NaSSBs on a commercial scale, five key factors will need to be addressed regarding the interface (see Table 10 for a summary of these barriers and corresponding solutions):

6.1. Na metal anode stability

While current research indicates that it is difficult to use a metallic

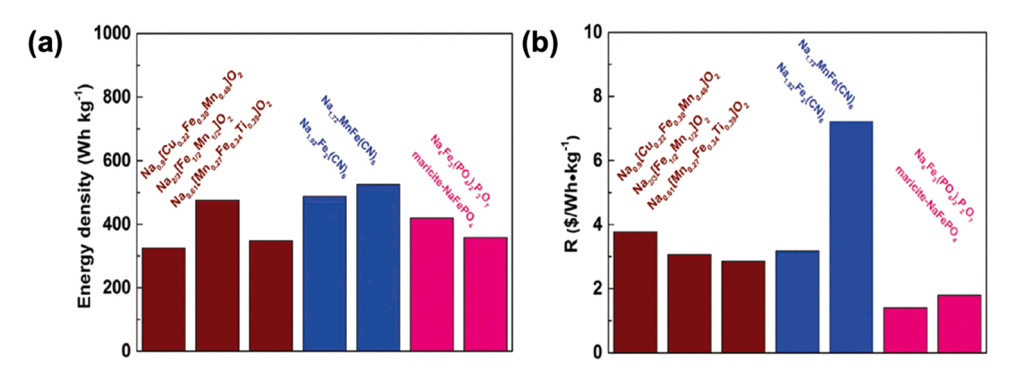


Fig. 15. Energy density (a) and cost per energy density (b) of select oxide (red), phosphate (pink), and hexacyanoferrate (blue) sodium cathodes. Reprinted (adapted) with permission from Li et al. [152]. Copyright 2017 Wiley.

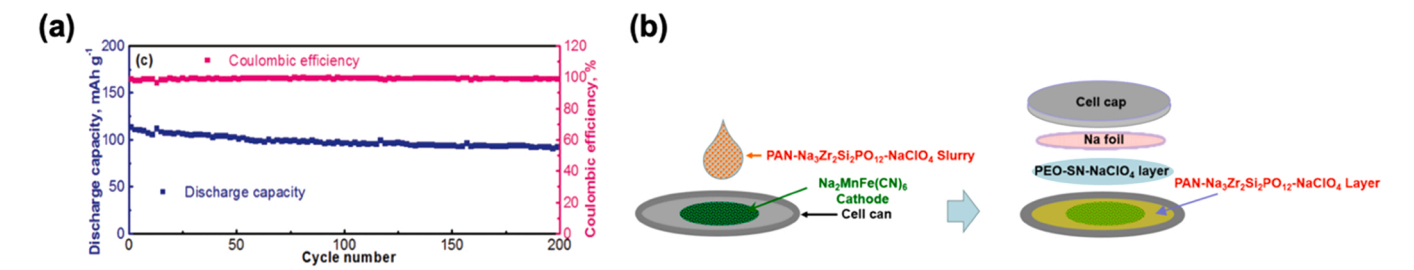


Fig. 16. (a) Galvanostatic cycling of NaSSB with laminate-type NaSE independently tuned for both cathode and anode and (b) assembly schematic of NaSSB with laminate-type NaSE.

Reprinted (adapted) with permission from Yu et al. [153]. Copyright 2020 Wiley.

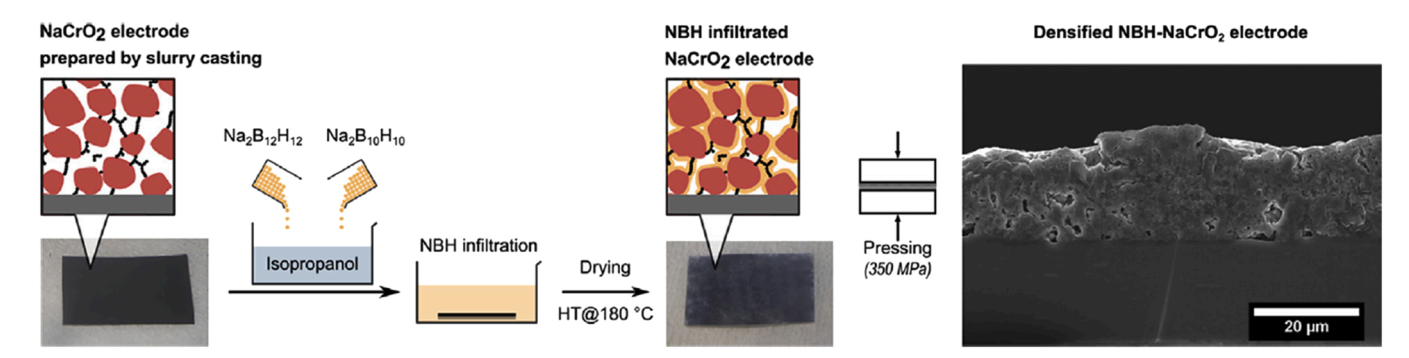


Fig. 17. Preparation and impregnation of NBH NaSE into NaCrO₂ cathode. (a) Reprinted from Duchêne et al. [154]. Copyright 2020, with permission from Elsevier.

sodium anode, the high energy density offered by this configuration is desirable for next-generation NaSSBs. Therefore, it is prudent to further investigate reactivity and electrode passivation at Na/SE interfaces, and ways to achieve intimate and robust bonding that can withstand extensive cycling. Anode wetting and buffer layer compatibility were discussed above and are good methods to achieve high contact areas and chemically-stable interfaces. However, to our knowledge, there is a lack of research on the use of buffer layers in half-cells, specifically at the Na/SE interface. Thus, this provides motivation to examine alternative buffer materials that could advance the configuration of NaSSBs.

6.2. Rate capability

Another key factor in developing NaSSBs is to improve the rate capability to meet the demands of high-power-density applications (e.g. electric vehicles). Hence, it is critical that NaSEs exhibit high Na $^+$ transference number ($\sim \! 1$) to mitigate the issue of electro-polarization during extensive cycling. In addition, it is desirable that NaSEs are stable at high critical current densities to enable fast charging. The target critical current density to compete against liquid electrolytes is $\sim 1{\text -}3~\text{mA}~\text{cm}^{\text -}2$. The microstructure and impurities of the NaSE is another parameter that could hinder the commercial application of NaSSBs.

6.3. Advances in cathode materials

With the assumption that Na metal is the anode of choice in highenergy NaSSBs, cathode optimization will determine maximum performance. To this end, Na-S systems offer higher capacities compared to oxide and phosphate counterparts. Advances in ambient, stable cycling with high material loadings will be key in commercializing S-based NaSSBs. Understanding advanced catholyte systems that maintain triple phase contact between active material, ionically-conductive and electronically-conductive additives is also of the utmost importance going forward.

6.4. Processability

While there are numerous electrolyte synthesis and processing methods, there are few commercially available for NaSSBs, which introduces concerns of scalability. Sulfide-based electrolytes, for instance, are highly moisture sensitive and could be difficult to produce on a large scale where the environment is less controlled. Other issues such as the generally brittle nature of oxide electrolytes can potentially be solved using the research directions given in this review, such as CPEs for creating a robust electrolyte with superior interfacial contact than the pure ceramic. Other methods that can be useful for creating facile contact with electrode materials include ionic liquid coatings, solution processing, and warm pressing.

6.5. Scalability for commercialization

For widespread use, a reliable and scalable battery storage system is required to meet the market demand. Selected efforts to accelerate the scale-up and commercialization of NaBs have been discussed above; however, extensive collaboration between researchers in multiple fields is mandated for further advances in transforming lab-scale materials to prototype levels. This includes optimization of the energy density and pack integration via electrode and cell design.

Author contributions

The manuscript was written with contributions from all authors.

Declaration of Competing Interest

The authors declare that they have no known competing financial interests or personal relationships that could have appeared to influence the work reported in this paper.

Table 9NaSSBs with a non-sulfur-based cathode.

Cell (cathode, electrolyte,	Reversible capacity, current density (mAh g ⁻¹ , mA g ⁻¹ or C-rate)	Interface Consideration	Ref.
anode)	, mag of c-rate)		
NVP-NZMSP, NZMSP-PEO- NaTFSI, Na metal	• 115.9 @ C/10	 NZMSP filler in PEO matrix increases CPE conductivity to 2.8 mS cm⁻¹ @ 80C. 	[75]
NVP-NZSP- sodiated Nafion, NZSP, Na metal	• 81.6 @ 20 mA g ⁻¹	 Sodiated Nafion used in composite NVP-NZSP cathode to ensure com- plete ionic contact be- tween cathode and NaSE. 	[150]
Na ₂ MnFe(CN) ₆ , PAN-NZSP- NaClO ₄ /PEO- SN-NaClO ₄ , Na metal	 91.9 @ C/5 after 200 cycles 125.4 @ C/20 	 Laminated composite electrolyte is used to best match to cathode (high voltage stability and dendrite protection) and anode (low voltage stability and increased Na⁺ conductivity). Both layers are required for improved performance and stability from 0 to 4.8 V vs. Na⁺/Na. 	[153]
NaCrO ₂ - Na ₃ SbO ₄ , Na ₃ SbO ₄ , Na- Sn	• 108 @ 50 μA cm ⁻²	 Solution-based Na₃SbO₄ enables direct coating of NaCrO₂ cathode particles for improved interface contact and performance. 	[58]
NaCrO ₂ -NBH, NBH, Na-Sn	• 118 @ C/2 • 80 @ 5 C	 NBH infiltration of NaCrO₂ cathode followed by subsequent pressing (70–350 MPa) allows for intimate ionic contact and current rates up to 5 C (4.5 mA cm⁻²). 	[154]
NVP@C, PEGDMA- NaFSI, Na metal	• 106 @ C/2 after 535 cycles	C coated NVP nanosheets paired with UV-cured, flexible SPE with NaFSI Na salt re- sults in stable interface and overall flexibility of cell.	[149]
NVP-PEO- NaTFSI, Ga- doped NZTO- PEO, Na metal	• 99 @ C/5 and 80C after 100 cycles	 PEO with dispersed NZTO reduces the polymer crystallization and greatly increases ionic conductivity while suppressing dendrite growth. PEO allows for soft interface. 	[155]
NVP, ETPTA- NaClO ₄ , Na metal	• 103 @ 1 C • 55 @ 15 C	 Highly flexible ETPTA-NaClO₄ quasi-solid NaSE offers ultra-high-rate capability up to 15 C due to RT ionic conductivity of 1.2 mS cm⁻¹, wide electro- chemical window. Coin and Pouch full-cells tested with similar performance. 	[151]
Na ₂ MnFe(CN) ₆ - PEO-NaClO ₄ , NZSP, Na metal	 120 @ C/2 89.2% retention after 200 cycles 	Cathode directly pressed onto NZSP pellet to ensure interfacial contact. Significantly less Mn dissolution measured in SE cell vs. liquid-electrolyte-based cell.	[156]

 $\begin{array}{lll} \textbf{NaTFSI} &= \text{Na}(\text{CF}_3\text{SO}_2)_2\text{N} \mid \textbf{NaFSI} = \text{sodium bis}(\text{fluorosulfonyl}) \text{ imide } \mid \textbf{NBH} \\ &= \text{Na}_4(\text{B}_{12}\text{H}_{12})(\text{B}_{10}\text{H}_{10}) \mid \textbf{NVP} = \text{Na}_3\text{V}_2(\text{PO}_4)_3 \mid \textbf{NZTO} = \text{Na}_2\text{Zn}_2\text{TeO}_6 \mid \textbf{PAN} \\ &= \text{poly}(\text{acrylonitrile}) \mid \textbf{PEO} = \text{polyethylene oxide} \mid \textbf{NZSP} = \text{Na}_3\text{Zr}_2\text{Si}_2\text{PO}_{12} \mid \textbf{NZMSP} = \text{Na}_{3,1}\text{Zr}_{1,95}\text{Mg}_{0.05}\text{Si}_2\text{PO}_{12} \mid \textbf{SN} = \text{succinonitrile} \mid \textbf{PEGDMA-NaFSI} \\ &= \text{CH}_3\text{O}(\text{CH}_2\text{CH}_2\text{O})_n\text{CH}_3 \mid \text{NaC}_2\text{F}_6\text{NO}_4\text{S}_2 \mid \textbf{ETPTA} = \text{trimethylolpropane ethoxylate triacrylate} \end{array}$

Table 10
Summary of key barriers for NaSSB interfaces and solutions to overcome them.

Barrier	Solutions				
	1	2	3		
Na anode stability	Investigate interfacial reactivity and electrode passivation	Surface and heat treatments for good wetting	Stable and high Na ⁺ diffusivity buffer layers		
Rate capability	High-transference- number electrolytes	More critical current density studies on NaSEs	High-purity NaSEs to increase conductivity		
Cathode materials	Further studies on Na-S at ambient	Studies of active material loading	High-ionic- conductivity catholytes		
Processability	Focus on feasible synthesis routes	Improve electrolyte mechanical properties (brittleness)	Use of interfacial modification		
Scalability	Studies on increasing NaSSB production from benchmark scale	Optimize energy density in pack design for NaSSBs	Optimize pack integration for electrodes and electrolyte		

Data Availability

No data was used for the research described in the article.

Acknowledgements

We are grateful for the support of a significant portion of this work by a gift from Mercedes-Benz Research & Development North America (MBRDNA). A portion of this work was also supported by a DMR NSF Grant No. DMR project 1926199.

Appendix A. Supporting information

Supplementary data associated with this article can be found in the online version at doi:10.1016/j.mtcomm.2022.104009.

References

- M. Hu, X. Pang, Z. Zhou, Recent progress in high-voltage lithium ion batteries, J. Power Sources 237 (2013) 229–242.
- [2] J.B. Goodenough, Y. Kim, Challenges for rechargeable Li batteries, Chem. Mater. 22 (3) (2010) 587–603.
- [3] N. Nitta, F. Wu, J.T. Lee, G. Yushin, Li-Ion battery materials: present and future, Mater. Today 18 (5) (2015) 252–264.
- [4] G. Zubi, R. Dufo-López, M. Carvalho, G. Pasaoglu, The lithium-ion battery: state of the art and future perspectives, Renew. Sustain. Energy Rev. 89 (2018) 202, 208
- [5] J. Wen, Y. Yu, C. Chen, A review on lithium-ion batteries safety issues: existing problems and possible solutions, Mater. Express (2012) 197–212, https://doi. org/10.1166/mex.2012.1075.
- [6] M.D. Slater, D. Kim, E. Lee, C.S. Johnson, Sodium-ion batteries, Adv. Funct. Mater. 23 (8) (2013) 947–958.
- [7] X. Lu, J.P. Lemmon, J.Y. Kim, V.L. Sprenkle, Z. Yang, High energy density Na–S/ NiCl2 hybrid battery, J. Power Sources 224 (Complete) (2013) 312–316, https://doi.org/10.1016/J.JPOWSOUR.2012.09.108.
- [8] D. Noel Buckley, C. O'Dwyer, N. Quill, R.P., Lynch, Electrochemical Energy Storage. Issues in Environmental Science and Technology. Royal Society of Chemistry October 15, 2019, pp 115–149. https://doi.org/10.1039/ 9781788015530–00115.

- [9] P.K. Nayak, L. Yang, W. Brehm, P. Adelhelm, From lithium-ion to sodium-ion batteries: advantages, challenges, and surprises, Angew. Chem. Int. Ed. 57 (1) (2018) 102–120, https://doi.org/10.1002/ANIE.201703772.
- [10] J.M. Tarascon, Is lithium the new gold? Nature chemistry, Nat. Publ. Group (2010) 510, https://doi.org/10.1038/nchem.680.
- [11] N. Tapia-Ruiz, A.R. Armstrong, H. Alptekin, M.A. Amores, H. Au, J. Barker, R. Boston, W.R. Brant, J.M. Brittain, Y. Chen, M. Chhowalla, Y.-S. Choi, S.I. R. Costa, M.C. Ribadeneyra, S.A. Cussen, E.J. Cussen, W.I.F. David, A.V. Desai, S. A.M. Dickson, E.I. Eweka, J.D. Forero-Saboya, C.P. Grey, J.M. Griffin, P. Gross, X. Hua, J.T.S. Irvine, P. Johansson, M.O. Jones, M. Karlsmo, E. Kendrick, E. Kim, O.V. Kolosov, Z. Li, S.F.L. Mertens, R. Mogensen, L. Monconduit, R.E. Morris, A. J. Naylor, S. Nikman, C.A. O'Keefe, D.M.C. Ould, R.G. Palgrave, P. Poizot, A. Ponrouch, S. Renault, E.M. Reynolds, A. Rudola, R. Sayers, D.O. Scanlon, S. Sen, V.R. Seymour, B. Silván, M.T. Sougrati, L. Stievano, G.S. Stone, C. I. Thomas, M.-M. Titirici, J. Tong, T.J. Wood, D.S. Wright, R. Younesi, Roadmap for sodium-ion batteries, J. Phys. Energy 2021 3 (3) (2021), 031503, https://doi.org/10.1088/2515-7655/AC01EF.
- [12] Y. Wang, S. Song, C. Xu, N. Hu, J. Molenda, L. Lu, Development of solid-state electrolytes for sodium-ion battery-a short review, Elem. Mineral. Soc. Am. June 1 (2021) 91–100, https://doi.org/10.1016/j.nanoms.2019.02.007.
- [13] P. Adelhelm, P. Hartmann, C.L. Bender, M. Busche, C. Eufinger, J. Janek, From lithium to sodium: cell chemistry of room temperature sodium-air and sodiumsulfur batteries, Beilstein J. Nanotechnol. 6 (1) (2015) 1016–1055, https://doi. org/10.3762/bjnano.6.105.
- [14] C. Zhao, L. Liu, X. Qi, Y. Lu, F. Wu, J. Zhao, Y. Yu, Y.-S. Hu, L. Chen, Solid-state sodium batteries, Adv. Energy Mater. 8 (17) (2018), 1703012, https://doi.org/ 10.1002/AFNM.201703012
- [15] N. Yabuuchi, K. Kubota, M. Dahbi, S. Komaba, Research development on sodiumion batteries, Chem. Rev. 114 (23) (2014) 11636–11682, https://doi.org/ 10.1021/CR500192F.
- [16] K. Vignarooban, R. Kushagra, A. Elango, P. Badami, B.E. Mellander, X. Xu, T. G. Tucker, C. Nam, A.M. Kannan, Current trends and future challenges of electrolytes for sodium-ion batteries, Int. J. Hydrog. Energy 41 (4) (2016) 2829–2846, https://doi.org/10.1016/j.ijhydene.2015.12.090.
- [17] K. Xu, S.P. Ding, T.R. Jow, Toward reliable values of electrochemical stability limits for electrolytes, J. Electrochem. Soc. 146 (11) (1999) 4172–4178, https://doi.org/10.1149/1.1392609.
- [18] B. Wu, S. Wang, W.J. Evans, D.Z. Deng, J. Yang, J. Xiao, Interfacial behaviours between lithium ion conductors and electrode materials in various battery systems, J. Mater. Chem. A. R. Soc. Chem. (2016) 15266–15280, https://doi.org/ 10.1039/c6ta05439k.
- [19] J.-J. Kim, K. Yoon, I. Park, K. Kang, Progress in the development of sodium-ion solid electrolytes, Small Methods 1 (10) (2017), 1700219, https://doi.org/ 10.1002/smtd.201700219.
- [20] N. Anantharamulu, K. Koteswara Rao, G. Rambabu, B. Vijaya Kumar, V. Radha, M. Vithal, A wide-ranging review on nasicon type materials, J. Mater. Sci. (2011) 2821–2837, https://doi.org/10.1007/s10853-011-5302-5.
- [21] J.Y. Hwang, S.T. Myung, Y.K. Sun, Sodium-ion batteries: present and future, Chem. Soc. Rev. R. Soc. Chem. June 21 (2017) 3529–3614, https://doi.org/ 10.1039/c6cs00776g.
- [22] J.W. Fergus, Ion transport in sodium ion conducting solid electrolytes, Solid State Ion. 227 (2012) 102–112, https://doi.org/10.1016/j.ssi.2012.09.019.
- [23] H. Pan, Y.S. Hu, L. Chen, Room-temperature stationary sodium-ion batteries for large-scale electric energy storage, Energy Environ. Sci. (2013) 2338–2360, https://doi.org/10.1039/c3ee40847g.
- [24] D. Kundu, E. Talaie, V. Duffort, L.F. Nazar, The emerging chemistry of sodium ion batteries for electrochemical energy storage, in: Angewandte Chemie -International Edition, 9, Wiley-VCH Verlag, March, 2015, pp. 3432–3448, https://doi.org/10.1002/anie.201410376.
- [25] G. Åvall, J. Mindemark, D. Brandell, P. Johansson, Sodium-ion battery electrolytes: modeling and simulations, Adv. Energy Mater. 8 (17) (2018), 1703036, https://doi.org/10.1002/aenm.201703036.
- [26] M. Sawicki, L.L. Shaw, Advances and challenges of sodium ion batteries as post lithium ion batteries, RSC Adv. 5 (65) (2015) 53129–53154, https://doi.org/ 10.1039/c5se083214
- [27] G.L. Xu, R. Amine, A. Abouimrane, H. Che, M. Dahbi, Z.F. Ma, I. Saadoune, J. Alami, W.L. Mattis, F. Pan, Z. Chen, K. Amine, Challenges in developing electrodes, electrolytes, and diagnostics tools to understand and advance sodiumion batteries, in: Advanced Energy Materials, 15, Wiley-VCH Verlag, 2018, https://doi.org/10.1002/aenm.201702403.
- [28] H. Che, S. Chen, Y. Xie, H. Wang, K. Amine, X.Z. Liao, Z.F. Ma, Electrolyte design strategies and research progress for room-temperature sodium-ion batteries, in: Energy and Environmental Science, 17, Royal Society of Chemistry, 2017, pp. 1075–1101, https://doi.org/10.1039/c7ee00524e.
- [29] H. Li, L. Ma, C. Han, Z. Wang, Z. Liu, Z. Tang, C. Zhi, Advanced rechargeable zinc-based batteries: recent progress and future perspectives, in: Nano Energy, 1, Elsevier Ltd, August, 2019, pp. 550–587, https://doi.org/10.1016/j.pp.2019.05.559
- [30] C.H. Dustmann, Advances in ZEBRA batteries, J. Power Sources (2004), https://doi.org/10.1016/j.jpowsour.2003.09.039.
- [31] X. Lu, G. Xia, J.P. Lemmon, Z. Yang, Advanced materials for sodium-beta alumina batteries: status, challenges and perspectives, J. Power Sources (2010), https:// doi.org/10.1016/j.jpowsour.2009.11.120.
- [32] J.F. Wu, R. Zhang, Q.F. Fu, J.S. Zhang, X.Y. Zhou, P. Gao, C.H. Xu, J. Liu, X. Guo, Inorganic solid electrolytes for all-solid-state sodium batteries: fundamentals and

- strategies for battery optimization, Adv. Funct. Mater. (2020), https://doi.org/
- [33] T. Famprikis, P. Canepa, J.A. Dawson, M.S. Islam, C. Masquelier, Fundamentals of Inorganic Solid-State Electrolytes for Batteries, Nat. Mater. (2019), https://doi. org/10.1038/s41563-019-0431-3.
- [34] Y. Zheng, Y. Yao, J. Ou, M. Li, D. Luo, H. Dou, Z. Li, K. Amine, A. Yu, Z. Chen, A review of composite solid-state electrolytes for lithium batteries: fundamentals, key materials and advanced structures, Chem. Soc. Rev. 49 (23) (2020) 8790–8839, https://doi.org/10.1039/D0CS00305K.
- [35] H. Tuller Ionic Conduction and Applications. In Springer Handbooks; 2017. https://doi.org/10.1007/978-3-319-48933-9_11.
- [36] Yung-Fang Yu Yao, J.T. Kummer, Ion exchange properties of and rates of ionic diffusion in beta-alumina, J. Inorg. Nucl. Chem. 29 (9) (1967) 2453–2475, https://doi.org/10.1016/0022-1902(67)80301-4.
- [37] J.B. Goodenough, H.Y.P. Hong, J.A. Kafalas, Fast Na+-Ion transport in skeleton structures, Mater. Res. Bull. 11 (2) (1976) 203–220, https://doi.org/10.1016/ 0025-5408(76)90077-5.
- [38] M.J. Rice, W.L. Roth, Ionic transport in super ionic conductors: a theoretical model, J. Solid State Chem. 4 (2) (1972) 294–310, https://doi.org/10.1016/ 0022-4596(72)90121-1.
- [39] A. Fukunaga, T. Nohira, Y. Kozawa, R. Hagiwara, S. Sakai, K. Nitta, S. Inazawa, Intermediate-temperature ionic liquid NaFSA-KFSA and Its Application to Sodium Secondary Batteries, J. Power Sources (2012), https://doi.org/10.1016/j. jpowsour.2012.02.058.
- [40] A.K. Ray, E.C. Subbarao, Synthesis of sodium β and B" alumina, Mater. Res. Bull. (1975), https://doi.org/10.1016/0025-5408(75)90186-5.
- [41] E. Yi, E. Temeche, R.M. Laine, Superionically conducting B"-Al2O3thin films processed using flame synthesized nanopowders, J. Mater. Chem. A (2018), https://doi.org/10.1039/c8ta02907e.
- [42] K.B. Hueso, M. Armand, T. Rojo, High temperature sodium batteries: status, challenges and future trends, in: Energy and Environmental Science, 20, The Royal Society of Chemistry, March, 2013, pp. 734–749, https://doi.org/10.1039/ c3ee24086j.
- [43] S. Liu, C. Zhou, Y. Wang, W. Wang, Y. Pei, J. Kieffer, R.M. Laine, Ce-substituted nanograin Na3Zr2Si2PO12 prepared by LF-FSP as sodium-ion conductors, ACS Appl. Mater. Interfaces (2020). https://doi.org/10.1021/acsami.9b11995.
- [44] H.Y.P. Hong, Crystal structures and crystal chemistry in the system Na1+ xZr2SixP3-X012, Mater. Res. Bull. (1976), https://doi.org/10.1016/0025-5408 (76)90073-8.
- [45] D. Xu, H. Jiang, M. Li, O. Hai, Y. Zhang, Synthesis and characterization of Y2O3 doped Na-B"-Al2O3 solid electrolyte by double zeta process, Ceram. Int. 41 (4) (2015) 5355–5361, https://doi.org/10.1016/j.ceramint.2014.12.094.
- [46] G. Chen, J. Lu, X. Zhou, L. Chen, X. Jiang, Solid-state synthesis of high performance Na-B"-Al2O3 solid electrolyte doped with MgO, Ceram. Int. 42 (14) (2016) 16055–16062, https://doi.org/10.1016/j.ceramint.2016.07.115.
- [47] S. Song, H.M. Duong, A.M. Korsunsky, N. Hu, L. Lu, A Na+ superionic conductor for room-temperature sodium batteries, Sci. Rep. 6 (1) (2016) 1–10, https://doi. org/10.1038/srep32330.
- [48] Q. Zhang, F. Liang, T. Qu, Y. Yao, W. Ma, B. Yang, Y. Dai, Effect on ionic conductivity of Na3+xZr2-XMxSi2PO12 (M=Y, La) by doping rare-earth elements, in: IOP Conference Series: Materials Science and Engineering, Vol. 423, Institute of Physics Publishing, 2018, https://doi.org/10.1088/1757-899X/423/1/012122
- [49] Y. Lu, J.A. Alonso, Q. Yi, L. Lu, Z. Lin Wang, C. Sun, Y. Lu, Q. Yi, L. Lu, Z.L. Wang, C. Sun, J.A. Alonso, A high-performance monolithic solid-state sodium battery with Ca2+ Doped Na3Zr2Si2PO12 electrolyte, Adv. Energy Mater. 9 (28) (2019), 1901205, https://doi.org/10.1002/AENM.201901205.
- [50] Z. Zhang, Q. Zhang, J. Shi, Y.S. Chu, X. Yu, K. Xu, M. Ge, H. Yan, W. Li, L. Gu, Y.-S. Hu, H. Li, X.-Q. Yang, L. Chen, X. Huang, A self-forming composite electrolyte for solid-state sodium battery with ultralong cycle life, Adv. Energy Mater. 7 (4) (2017), 1601196, https://doi.org/10.1002/aenm.201601196.
- [51] B. Tang, P.W. Jaschin, X. Li, S.H. Bo, Z. Zhou, Critical interface between inorganic solid-state electrolyte and sodium metal, Mater. Today (2020), https://doi.org/ 10.1016/j.mattod.2020.08.016.
- [52] E. Matios, H. Wang, C. Wang, W. Li, Enabling safe sodium metal batteries by solid electrolyte interphase engineering: a review, Ind. Eng. Chem. Res. (2019), https://doi.org/10.1021/acs.iecr.9b02029.
- [53] C. Bao, B. Wang, P. Liu, H. Wu, Y. Zhou, D. Wang, H. Liu, S. Dou, Solid electrolyte interphases on sodium metal anodes, Adv. Funct. Mater. (2020), https://doi.org/ 10.1002/adfm.202004891.
- [54] A. Hayashi, K. Noi, N. Tanibata, M. Nagao, M. Tatsumisago, High sodium ion conductivity of glass-ceramic electrolytes with cubic Na3PS4, J. Power Sources 258 (2014) 420–423, https://doi.org/10.1016/j.jpowsour.2014.02.054.
- [55] Z. Yu, S.-L. Shang, J.-H. Seo, D. Wang, X. Luo, Q. Huang, S. Chen, J. Lu, X. Li, Z.-K. Liu, D. Wang, Exceptionally high ionic conductivity in Na₃ P_{0.62} As_{0.38} S₄ with improved moisture stability for solid-state sodium-ion batteries, Adv. Mater. 29 (16) (2017), 1605561, https://doi.org/10.1002/adma.201605561.
- [56] A. Hayashi, K. Noi, A. Sakuda, M. Tatsumisago, Superionic glass-ceramic electrolytes for room-temperature rechargeable sodium batteries, Nat. Commun. (2012), https://doi.org/10.1038/ncomms1843.
- [57] M. Jansen, U. Henseler, Synthesis, structure determination, and ionic conductivity of sodium tetrathiophosphate, J. Solid State Chem. (1992), https://doi.org/10.1016/0022-4596(92)90295-7.
- [58] A. Banerjee, K.H. Park, J.W. Heo, Y.J. Nam, C.K. Moon, S.M. Oh, S.T. Hong, Y. S. Jung, Na3SbS4: a solution processable sodium superionic conductor for all-

- solid-state sodium-ion batteries, Angew. Chem. Int. Ed. (2016), https://doi.org/
- [59] W.D. Richards, T. Tsujimura, L.J. Miara, Y. Wang, J.C. Kim, S.P. Ong, I. Uechi, N. Suzuki, G. Ceder, Design and synthesis of the superionic conductor Na 10 SnP 2 S 12, Nat. Commun. 7 (1) (2016) 1–8, https://doi.org/10.1038/ncomms11009.
- [60] M. Duchardt, U. Ruschewitz, S. Adams, S. Dehnen, B. Roling, Vacancy-controlled Na+ superion conduction in Na11Sn2PS12, Angew. Chem. - Int. Ed. 57 (5) (2018) 1351–1355, https://doi.org/10.1002/ANIE.201712769.
- [61] H. Gamo, H.H.P. Nguyen, R. Matsuda, H. Muto, A. Matsuda, Na3+x(Sb1-XSnx)S4 solid electrolytes (0 ≤ x ≤ 0.1) as sodium ion conductors, Solid State Ion. 344 (2020), 115133, https://doi.org/10.1016/J.SSI.2019.115133.
- [62] L. Zhang, K. Yang, J. Mi, L. Lu, L. Zhao, L. Wang, Y. Li, H. Zeng, Na3PSe4: a novel chalcogenide solid electrolyte with high ionic conductivity, Adv. Energy Mater. 5 (24) (2015), 1501294, https://doi.org/10.1002/AENM.201501294.
- [63] D. Zhang, X. Cao, D. Xu, N. Wang, C. Yu, W. Hu, X. Yan, J. Mi, B. Wen, L. Wang, L. Zhang, Synthesis of cubic Na3SbS4 solid electrolyte with enhanced ion transport for all-solid-state sodium-ion batteries, Electrochim. Acta 259 (2018) 100–109, https://doi.org/10.1016/j.electacta.2017.10.173.
- [64] V.S. Kandagal, M.D. Bharadwaj, U.V. Waghmare, Theoretical prediction of a highly conducting solid electrolyte for sodium batteries: Na10GeP2S12, J. Mater. Chem. A 3 (24) (2015) 12992–12999, https://doi.org/10.1039/c5ta01616a.
- [65] I.H. Chu, C.S. Kompella, H. Nguyen, Z. Zhu, S. Hy, Z. Deng, Y.S. Meng, S.P. Ong, Room-temperature all-solid-state rechargeable sodium-ion batteries with a Cl-Doped Na 3 PS 4Superionic Conductor, Sci. Rep. 6 (1) (2016) 1–10, https://doi. org/10.1038/srep33733.
- [66] H. Oguchi, M. Matsuo, S. Kuromoto, H. Kuwano, S. Orimo, Sodium-ion conduction in complex hydrides NaAlH4 and Na3AlH6, J. Appl. Phys. 111 (3) (2012), 036102, https://doi.org/10.1063/1.3681362.
- [67] M. Matsuo, H. Oguchi, T. Sato, H. Takamura, E. Tsuchida, T. Ikeshoji, S.I. Orimo, Sodium and magnesium ionic conduction in complex hydrides, J. Alloy. Compd. SUPPL1 (2013) 580, https://doi.org/10.1016/J.JALLCOM.2013.01.058.
- [68] T.J. Udovic, M. Matsuo, A. Unemoto, N. Verdal, V. Stavila, A.V. Skripov, J. J. Rush, H. Takamura, S.I. Orimo, Sodium superionic conduction in Na2B12H12, Chem. Commun. 50 (28) (2014) 3750–3752, https://doi.org/10.1039/C3CC49805K.
- [69] M. Dimitrievska, P. Shea, K.E. Kweon, M. Bercx, J.B. Varley, W.S. Tang, A. V. Skripov, V. Stavila, T.J. Udovic, B.C. Wood, Carbon incorporation and anion dynamics as synergistic drivers for ultrafast diffusion in superionic LiCB11H12 and NaCB11H12, Adv. Energy Mater. 8 (15) (2018), 1703422, https://doi.org/10.1002/AENM.201703422.
- [70] W.S. Tang, K. Yoshida, A.V. Soloninin, R.V. Skoryunov, O.A. Babanova, A. V. Skripov, M. Dimitrievska, V. Stavila, S.I. Orimo, T.J. Udovic, Stabilizing superionic-conducting structures via mixed-anion solid solutions of monocarbacloso-borate salts, ACS Energy Lett. 1 (4) (2016) 659–664, https://doi.org/10.1021/ACSENERGYLETT.6B00310/ASSET/IMAGES/LARGE/NZ-2016-00310Y 0004_JPEG.
- [71] Y. Qie, S. Wang, S. Fu, H. Xie, Q. Sun, P. Jena, Yttrium-sodium halides as promising solid-state electrolytes with high ionic conductivity and stability for Na-Ion batteries, J. Phys. Chem. Lett. 11 (9) (2020) 3376–3383, https://doi.org/ 10.1021/ACS.JPCLETT.0C00010/SUPPL_FILE/JZ0C00010_SI_001.PDF.
- [72] W.G. Zeier, R. Schlem, A. Banik, M. Eckardt, M. Zobel, Na3—xEr1—xZrxCl6-a halide-based fast sodium-ion conductor with vacancy-driven ionic transport, ACS Appl. Energy Mater. 3 (10) (2020) 10164–10173, https://doi.org/10.1021/ ACSAEM.0C01870/SUPPL FILE/AE0C01870 SI 001.PDF.
- [73] E.A. Wu, S. Banerjee, H. Tang, P.M. Richardson, J.M. Doux, J. Qi, Z. Zhu, A. Grenier, Y. Li, E. Zhao, G. Deysher, E. Sebti, H. Nguyen, R. Stephens, G. Verbist, K.W. Chapman, R.J. Clément, A. Banerjee, Y.S. Meng, S.P. Ong, A stable cathode-solid electrolyte composite for high-voltage, long-cycle-life solid-state sodium-ion batteries, Nat. Commun. 2021 121 12 (1) (2021) 1–11, https://doi.org/10.1038/s41467-021-21488-7.
- [74] Z. Zhang, Q. Zhang, C. Ren, F. Luo, Q. Ma, Y.S. Hu, Z. Zhou, H. Li, X. Huang, L. Chen, A ceramic/polymer composite solid electrolyte for sodium batteries, J. Mater. Chem. A 4 (41) (2016) 15823–15828, https://doi.org/10.1039/ 05007500h
- [75] Z. Zhang, K. Xu, X. Rong, Y.S. Hu, H. Li, X. Huang, L. Chen, Na3.4Zr1.8Mg0.2Si2PO12 filled poly(Ethylene Oxide)/Na(CF3SO2)2N as flexible composite polymer electrolyte for solid-state sodium batteries, J. Power Sources 372 (2017) 270–275, https://doi.org/10.1016/j.jpowsour.2017.10.083.
- [76] L. Long, S. Wang, M. Xiao, Y. Meng, Polymer electrolytes for lithium polymer batteries, J. Mater. Chem. A (2016), https://doi.org/10.1039/c6ta02621d.
- [77] J. Yang, H. Zhang, Q. Zhou, H. Qu, T. Dong, M. Zhang, B. Tang, J. Zhang, G. Cui, Safety-enhanced polymer electrolytes for sodium batteries: recent progress and perspectives, ACS Appl. Mater. Interfaces (2019), https://doi.org/10.1021/ acsami.9b01239.
- [78] D.T. Hallinan, N.P. Balsara, Polymer electrolytes, Annu. Rev. Mater. Res. (2013), https://doi.org/10.1146/annurev-matsci-071312-121705.
- [79] D.E. Fenton, J.M. Parker, P.V. Wright, Complexes of alkali metal ions with poly (ethylene oxide, Polym. (Guildf.) (1973), https://doi.org/10.1016/0032-3861 (73)00146.8
- [80] R.C. Agrawal, G.P. Pandey, Solid polymer electrolytes: materials designing and all-solid-state battery applications: an overview, J. Phys. D. Appl. Phys. (2008), https://doi.org/10.1088/0022-3727/41/22/223001.
- [81] Y. Zhao, Y. Zhang, D. Gosselink, T.N.L. Doan, M. Sadhu, H.J. Cheang, P. Chen, Polymer electrolytes for lithium/sulfur batteries, Membranes (2012), https://doi. org/10.3390/membranes2030553.

- [82] N.A. Stolwijk, C. Heddier, M. Reschke, M. Wiencierz, J. Bokeloh, G. Wilde, Salt-concentration dependence of the glass transition temperature in PEO-NaI and PEO-LiTFSI polymer electrolytes, Macromolecules (2013), https://doi.org/10.1021/ma401686r
- [83] K.E. Strawhecker, E. Manias, Crystallization behavior of poly(ethylene oxide) in the presence Of Na+ montmorillonite fillers, Chem. Mater. (2003), https://doi. org/10.1021/cm0212865.
- [84] E. Temeche, X. Zhang, R.M. Laine, Solid electrolytes for Li–S batteries: solid solutions of poly(ethylene oxide) with LixPON- and LixSiPON-based polymers, ACS Appl. Mater. Interfaces (2020), https://doi.org/10.1021/acsami.0c06196.
- [85] W. Wang, E. Yi, A.J. Fici, R.M. Laine, J. Kieffer, Lithium ion conducting poly (ethylene oxide)-based solid electrolytes containing active or passive ceramic nanoparticles, J. Phys. Chem. C. 121 (5) (2017) 2563–2573, https://doi.org/ 10.1021/acs.ipcc.6b11136.
- [86] N. Angulakshmi, K.S. Nahm, V. Swaminathan, S. Thomas, R. Nimma Elizabeth, Nanocomposite polymer electrolytes for lithium batteries, Polym. Process. Charact. (2012), https://doi.org/10.1201/b13105.
- [87] M. Dinachandra Singh, A. Dalvi, D.M. Phase, Electrical transport in PEO-NaI-NASICON nanocomposites: an assessment using impedance and X-Ray absorption spectroscopy, Mater. Res. Bull. (2019), https://doi.org/10.1016/j.materresbull 2019 05 010
- [88] C. Sångeland, R. Younesi, J. Mindemark, D. Brandell, Towards room temperature operation of all-solid-state na-ion batteries through polyester–polycarbonatebased polymer electrolytes, Energy Storage Mater. 19 (2019) 31–38, https://doi. org/10.1016/J.ENSM.2019.03.022.
- [89] E. Matios, H. Wang, J. Luo, Y. Zhang, C. Wang, X. Lu, X. Hu, Y. Xu, W. Li, Reactivity-guided formulation of composite solid polymer electrolytes for superior sodium metal batteries, J. Mater. Chem. A 9 (34) (2021) 18632–18643, https://doi.org/10.1039/D1TA05490B.
- [90] M.D. Singh, A. Dalvi, Novel hybrid composites NaCF3SO3-PEO-NASICON for sodium ion battery applications, in: AIP Conference Proceedings, Vol. 2115, American Institute of Physics Inc., 2019, https://doi.org/10.1063/1.5113404.
- [91] X. Yu, L. Xue, J.B. Goodenough, A. Manthiram, A high-performance all-solid-state sodium battery with a poly(ethylene oxide)-Na3Zr2Si2PO12 composite electrolyte, ACS Mater. Lett. 1 (1) (2019) 132–138, https://doi.org/10.1021/ acsmaterialslett.9b00103.
- [92] D. Lei, Y.B. He, H. Huang, Y. Yuan, G. Zhong, Q. Zhao, X. Hao, D. Zhang, C. Lai, S. Zhang, J. Ma, Y. Wei, Q. Yu, W. Lv, Y. Yu, B. Li, Q.H. Yang, Y. Yang, J. Lu, F. Kang, Cross-linked beta alumina nanowires with compact gel polymer electrolyte coating for ultra-stable sodium metal battery, Nat. Commun. 10 (1) (2019) 1–11.
- [93] H. Tang, Z. Deng, Z. Lin, Z. Wang, I.H. Chu, C. Chen, Z. Zhu, C. Zheng, S.P. Ong, Probing solid-solid interfacial reactions in all-solid-state sodium-ion batteries with first-principles calculations, Chem. Mater. 30 (1) (2018) 163–173, https://doi.org/10.1021/acs.chemmater.7b04096.
- [94] D.K. Maurya, R. Dhanusuraman, Z. Guo, S. Angaiah, Composite polymer electrolytes: progress, challenges, and future outlook for sodium-ion batteries, Adv. Compos. Hybrid. Mater. (2022), https://doi.org/10.1007/S42114-021-00412-7.
- [95] Z. Zhang, Q. Zhang, Q. Ma, C. Ren, F. Luo, Y.-S. Hu, Z. Zhou, H. Li, X. Huang, L. Chen, A ceramic/polymer composite solid electrolyte for sodium batteries sodium-ion batteries, Artic. J. Mater. Chem. A (2016), https://doi.org/10.1039/ C6TA07590H
- [96] A.M. Stephan, Review on gel polymer electrolytes for lithium batteries, Eur. Polym. J. (2006), https://doi.org/10.1016/j.eurpolymj.2005.09.017.
- [97] H. Gao, B. Guo, J. Song, K. Park, J.B. Goodenough, A composite gel-polymer/glass-fiber electrolyte for sodium-ion batteries, Adv. Energy Mater. (2015), https://doi.org/10.1002/aenm.201402235.
- [98] J. Kim, II, Y. Choi, K.Y. Chung, J.H. Park, A structurable gel-polymer electrolyte for sodium ion batteries, Adv. Funct. Mater. (2017), https://doi.org/10.1002/ adfm 201701768
- [99] S.A. Hashmi, M.Y. Bhat, M.K. Singh, N.T.K. Sundaram, B.P.C. Raghupathy, H. Tanaka, Ionic liquid-based sodium ion-conducting composite gel polymer electrolytes: effect of active and passive fillers, J. Solid State Electrochem (2016), https://doi.org/10.1007/s10008-016-3284-6.
- [100] Y. Huang, L. Zhao, L. Li, M. Xie, F. Wu, R. Chen, Electrolytes and electrolyte/ electrode interfaces in sodium-ion batteries: from scientific research to practical application, Adv. Mater. 31 (21) (2019), 1808393, https://doi.org/10.1002/ adma.201808393.
- [101] C. Bommier, X. Ji, Electrolytes, SEI formation, and binders: a review of nonelectrode factors for sodium-ion battery anodes, Small 14 (16) (2018), 1703576, https://doi.org/10.1002/smll.201703576.
- [102] J. Yue, X. Zhu, F. Han, X. Fan, L. Wang, J. Yang, C. Wang, Long cycle life all-solid-state sodium ion battery, ACS Appl. Mater. Interfaces 10 (46) (2018) 39645–39650, https://doi.org/10.1021/acsami.8b12610.
- [103] W. Zhou, Y. Li, S. Xin, J.B. Goodenough, Rechargeable sodium all-solid-state battery, ACS Cent. Sci. 3 (1) (2017) 52–57, https://doi.org/10.1021/ acscentsci.6b00321.
- [104] H.J. Chang, X. Lu, J.F. Bonnett, N.L. Canfield, K. Han, M.H. Engelhard, K. Jung, V. L. Sprenkle, G. Li, Decorating β"-alumina solid-state electrolytes with micron Pb spherical particles for improving na wettability at lower temperatures, J. Mater. Chem. A 6 (40) (2018) 19703–19711, https://doi.org/10.1039/c8ta06745g.
- [105] M. Bay, M. Wang, R. Grissa, M.V.F. Heinz, J. Sakamoto, C. Battaglia, Sodium plating from Na-β"-alumina ceramics at room temperature, paving the way for fast-charging all-solid-state batteries, Adv. Energy Mater. 10 (3) (2020), 1902899, https://doi.org/10.1002/aenm.201902899.

- [106] Y. You, A. Manthiram, Progress in high-voltage cathode materials for rechargeable sodium-ion batteries, Adv. Energy Mater. Wiley-VCH Verl. (2018), https://doi.org/10.1002/aenm.201701785.
- [107] R. Asakura, D. Reber, L. Duchêne, S. Payandeh, A. Remhof, H. Hagemann, C. Battaglia, 4 V room-temperature all-solid-state sodium battery enabled by a passivating cathode/hydroborate solid electrolyte interface, Energy Environ. Sci. 13 (12) (2020) 5048–5058, https://doi.org/10.1039/D0EE01569E.
- [108] L. Duchène, R.S. Kühnel, E. Stilp, E. Cuervo Reyes, A. Remhof, H. Hagemann, C. Battaglia, A stable 3 v all-solid-state sodium-ion battery based on a closo-borate electrolyte, Energy Environ. Sci. 10 (12) (2017) 2609–2615, https://doi.org/ 10.1039/c7ee02420g.
- [109] K.H. Park, D.Y. Oh, Y.E. Choi, Y.J. Nam, L. Han, J.Y. Kim, H. Xin, F. Lin, S.M. Oh, Y.S. Jung, Solution-processable glass Lil-Li4SnS4 superionic conductors for all-solid-state Li-Ion batteries, Adv. Mater. 28 (9) (2016) 1874–1883, https://doi.org/10.1002/adma.201505008.
- [110] A. Inoishi, T. Omuta, E. Kobayashi, A. Kitajou, S. Okada, A single-phase, all-solid-state sodium battery using Na 3-x V 2-x Zr_x (PO₄) 3 as the cathode, anode, and electrolyte, Adv. Mater. Interfaces 4 (5) (2017), 1600942, https://doi.org/10.1002/admi.2016.0042
- [111] F. Lalère, J.B. Leriche, M. Courty, S. Boulineau, V. Viallet, C. Masquelier, V. Seznec, An all-solid state NASICON sodium battery operating at 200°C, J. Power Sources 247 (2014) 975–980, https://doi.org/10.1016/j. inowsour.2013.09.051.
- [112] T. Wei, Y. Gong, X. Zhao, K. Huang, An all-ceramic solid-state rechargeable Na +battery operated at intermediate temperatures, Adv. Funct. Mater. 24 (34) (2014) 5380-5384, https://doi.org/10.1002/adfm.201400773.
- [113] E. Jeong, C. Hong, Y. Tak, S.C. Nam, S. Cho, Investigation of interfacial resistance between LiCoO2 cathode and LiPON electrolyte in the thin film battery, J. Power Sources 159 (1 SPEC. ISS.) (2006) 223–226, https://doi.org/10.1016/j. jpowsour.2006.04.042.
- [114] K.H. Kim, Y. Iriyama, K. Yamamoto, S. Kumazaki, T. Asaka, K. Tanabe, C.A. J. Fisher, T. Hirayama, R. Murugan, Z. Ogumi, Characterization of the interface between LiCoO2 and Li 7La3Zr2O12 in an all-solid-state rechargeable lithium battery, J. Power Sources 196 (2) (2011) 764–767, https://doi.org/10.1016/j.ipowsour.2010.07.073.
- [115] T. Kobayashi, A. Yamada, R. Kanno, Interfacial reactions at electrode/electrolyte boundary in all solid-state lithium battery using inorganic solid electrolyte, Thio-LISICON, Electrochim. Acta 53 (15) (2008) 5045–5050, https://doi.org/10.1016/ i.electacta.2008.01.071.
- [116] A. Sakuda, A. Hayashi, M. Tatsumisago, Interfacial observation between LiCoO2 electrode and Li 25-P2S5 solid electrolytes of all-solid-state lithium secondary batteries using transmission electron microscopy, Chem. Mater. 22 (3) (2010) 949–956. https://doi.org/10.1021/cm901819c.
- [117] Y. Noguchi, E. Kobayashi, L.S. Plashnitsa, S. Okada, J.I. Yamaki, Fabrication and performances of all solid-state symmetric sodium battery based on NASICONrelated compounds, Electrochim. Acta 101 (2013) 59–65, https://doi.org/ 10.1016/j.electacta.2012.11.038.
- [118] B. Ahmed, D.H. Anjum, M.N. Hedhili, H.N. Alshareef, Mechanistic insight into the stability of HfO 2 -coated MoS 2 nanosheet anodes for sodium ion batteries, Small 11 (34) (2015) 4341–4350, https://doi.org/10.1002/smll.201500919.
- [119] X. Yu, A. Manthiram, Sodium-sulfur batteries with a polymer-coated NASICON-type sodium-ion solid electrolyte, Matter 1 (2) (2019) 439–451, https://doi.org/10.1016/j.matt.2019.03.008.
- [120] L. Liu, X. Qi, Q. Ma, X. Rong, Y.S. Hu, Z. Zhou, H. Li, X. Huang, L. Chen, Toothpaste-like electrode: a novel approach to optimize the interface for solidstate sodium-ion batteries with ultralong cycle life, ACS Appl. Mater. Interfaces 8 (48) (2016) 23631–23636. https://doi.org/10.1031/acseptib.11773
- (48) (2016) 32631–32636, https://doi.org/10.1021/acsami.6b11773.
 [121] X. Xu, L. Si, X. Zhou, F. Tu, X. Zhu, J. Bao, Chemical bonding between antimony and ionic liquid-derived nitrogen-doped carbon for sodium-ion battery anode, J. Power Sources 349 (2017) 37–44, https://doi.org/10.1016/j.jowsour.2017.03.026.
- [122] Ionotec beta alumina supplier-Conductive ceramics and beta alumina supplier http://www.ionotec.com/ (accessed Oct 4, 2021).
- [123] S. Wenzel, H. Metelmann, C. Raiß, A.K. Dürr, J. Janek, P. Adelhelm, Thermodynamics and cell chemistry of room temperature sodium/sulfur cells with liquid and liquid/solid electrolyte, J. Power Sources (2013), https://doi.org/ 10.1016/j.jpowsour.2013.05.194.
- [124] B. Jinisha, K.M. Anilkumar, M. Manoj, A. Abhilash, V.S. Pradeep, S. Jayalekshmi, Poly (ethylene oxide) (PEO)-based, sodium ion-conducting, solid polymer electrolyte films, dispersed with Al2O3 filler, for applications in sodium ion cells, Ion. (Kiel.) 24 (6) (2018) 1675–1683, https://doi.org/10.1007/s11581-017-2332-2.
- [125] P.S. Anantha, K. Hariharan, Physical and ionic transport studies on poly(ethylene oxide)-NaNO 3 polymer electrolyte system, Solid State Ion. 176 (1–2) (2005) 155–162, https://doi.org/10.1016/j.ssi.2004.07.006.
- [126] Y. Tian, T. Shi, W.D. Richards, J. Li, J.C. Kim, S.H. Bo, G. Ceder, Compatibility issues between electrodes and electrolytes in solid-state batteries, Energy Environ. Sci. 10 (5) (2017) 1150–1166, https://doi.org/10.1039/c7ee00534b.
- [127] S. Bag, C. Zhou, S. Reid, S. Butler, V. Thangadurai, Electrochemical studies on symmetric solid-state Na-ion full cell using Na3V2(PO4)3 electrodes and polymer composite electrolyte, J. Power Sources 454 (2020), 227954, https://doi.org/ 10.1016/j.jpowsour.2020.227954.
- [128] Y. Uchida, G. Hasegawa, K. Shima, M. Inada, N. Enomoto, H. Akamatsu, K. Hayashi, Insights into sodium ion transfer At The Na/NASICON interface improved by uniaxial compression, ACS Appl. Energy Mater. 2 (4) (2019) 2913–2920, https://doi.org/10.1021/acsaem.9b00250.

- [129] Q. Ma, C.L. Tsai, X.K. Wei, M. Heggen, F. Tietz, J.T.S. Irvine, Room temperature demonstration of a sodium superionic conductor with grain conductivity in excess of 0.01 S Cm-1 and its primary applications in symmetric battery cells, J. Mater. Chem. A 7 (13) (2019) 7766–7776, https://doi.org/10.1039/c9ta00048h.
- [130] H. Fu, Q. Yin, Y. Huang, H. Sun, Y. Chen, R. Zhang, Q. Yu, L. Gu, J. Duan, W. Luo, Reducing interfacial resistance by Na-SiO2 composite anode for NASICON-based solid-state sodium battery, ACS Mater. Lett. 2 (2) (2020) 127–132, https://doi. org/10.1021/acsmaterialslett.9b00442.
- [131] L. Duchêne, R.S. Kühnel, D. Rentsch, A. Remhof, H. Hagemann, C. Battaglia, A highly stable sodium solid-state electrolyte based on a dodeca/deca-borate equimolar mixture, Chem. Commun. 53 (30) (2017) 4195–4198, https://doi.org/ 10.1039/c7rc00704a
- [132] Y. Wang, Z. Wang, J. Sun, F. Zheng, M. Kotobuki, T. Wu, K. Zeng, L. Lu, Flexible, stable, fast-ion-conducting composite electrolyte composed of nanostructured Nasuper-ion-conductor framework and continuous poly(ethylene oxide) for all-solid-state na battery, J. Power Sources 454 (2020), 227949, https://doi.org/10.1016/ J.POWSOUR. 2020. 227949.
- [133] L.S. Plashnitsa, E. Kobayashi, Y. Noguchi, S. Okada, J. Yamaki, Performance of NASICON symmetric cell with ionic liquid electrolyte, J. Electrochem. Soc. 157 (4) (2010) A536, https://doi.org/10.1149/1.3298903.
- [134] X. Xu, D. Zhou, X. Qin, K. Lin, F. Kang, B. Li, D. Shanmukaraj, T. Rojo, M. Armand, G. Wang, A room-temperature sodium-sulfur battery with high capacity and stable cycling performance, Nat. Commun. 9 (1) (2018), https://doi.org/ 10.1038/s41467-018-06443-3.
- [135] Y. Lyu, Y. Liu, Z.E. Yu, N. Su, Y. Liu, W. Li, Q. Li, B. Guo, B. Liu, Recent advances in high energy-density cathode materials for sodium-ion batteries, Sustain. Mater. Technol. (2019) 21, https://doi.org/10.1016/J.SUSMAT.2019.E00098.
- [136] Y. Wang, D. Zhou, V. Palomares, D. Shanmukaraj, B. Sun, X. Tang, C. Wang, M. Armand, T. Rojo, G. Wang, Revitalising sodium-sulfur batteries for non-high-temperature operation: a crucial review, Energy Environ. Sci. R. Soc. Chem.. 1 (2020) 3848–3879, https://doi.org/10.1039/d0ee02203a.
- [137] I. Kim, J.Y. Park, C.H. Kim, J.W. Park, J.P. Ahn, J.H. Ahn, K.W. Kim, H.J. Ahn, A room temperature Na/S battery using a B" alumina solid electrolyte separator, tetraethylene glycol dimethyl ether electrolyte, and a S/C composite cathode, J. Power Sources 301 (2016) 332–337, https://doi.org/10.1016/j.ioowsour.2015.09.120.
- [138] C.W. Park, H.S. Ryu, K.W. Kim, J.H. Ahn, J.Y. Lee, H.J. Ahn, Discharge properties of all-solid sodium-sulfur battery using poly (ethylene oxide) electrolyte, J. Power Sources 165 (1) (2007) 450–454, https://doi.org/10.1016/j. ipowsour.2006.11.083.
- [139] C. Yu, S. Ganapathy, N.J.J. De Klerk, E.R.H. Van Eck, M. Wagemaker, Na-Ion dynamics in tetragonal and cubic Na3PS4, a Na-Ion conductor for solid state Na-Ion batteries, J. Mater. Chem. A 4 (39) (2016) 15095–15105, https://doi.org/ 10.1039/cfta058966
- [140] J. Kim, S.H. Jo, S. Bhavaraju, A. Eccleston, S.O. Kang, Low temperature performance of sodium-nickel chloride batteries with NaSICON solid electrolyte, J. Electronal. Chem. 759 (2015) 201–206, https://doi.org/10.1016/j. ielectem 2015 11 022
- [141] J. Yue, F. Han, X. Fan, X. Zhu, Z. Ma, J. Yang, C. Wang, High-performance all-inorganic solid-state sodium-sulfur battery, ACS Nano 11 (5) (2017) 4885–4891, https://doi.org/10.1021/acsnano.7b01445.
- [142] H. Wan, W. Weng, F. Han, L. Cai, C. Wang, X. Yao, Bio-inspired nanoscaled electronic/ionic conduction networks for room-temperature all-solid-state sodium-sulfur battery, Nano Today (2020) 33, https://doi.org/10.1016/j. nantod/2020.100860
- [143] T. Ando, A. Sakuda, M. Tatsumisago, A. Hayashi, All-solid-state sodium-sulfur battery showing full capacity with activated carbon MSP20-sulfur-Na35bS4 composite, Electrochem. Commun. (2020) 116, https://doi.org/10.1016/j. elecom.2020.106741.
- [144] T. Zhu, X. Dong, Y. Liu, Y.G. Wang, C. Wang, Y.Y. Xia, An all-solid-state sodium-sulfur battery using a sulfur/carbonized polyacrylonitrile composite cathode, ACS Appl. Energy Mater. 2 (7) (2019) 5263–5271, https://doi.org/10.1021/acsaem_9b00953
- [145] D. Zhou, Y. Chen, B. Li, H. Fan, F. Cheng, D. Shanmukaraj, T. Rojo, M. Armand, G. Wang, A stable quasi-solid-state sodium-sulfur battery, Angew. Chem. 130 (32) (2018) 10325–10329, https://doi.org/10.1002/ange.201805008.
- [146] Z. Ge, J. Li, J. Liu, Enhanced electrochemical performance of all-solid-state sodium-sulfur batteries by PEO-NaCF3SO3-MIL-53(Al) solid electrolyte, Ion. (Kiel.) 26 (4) (2020) 1787–1795, https://doi.org/10.1007/s11581-020-03513-9.
- [147] X. Xu, Y. Li, J. Cheng, G. Hou, X. Nie, Q. Ai, L. Dai, J. Feng, L. Ci, Composite solid electrolyte of Na3PS4-PEO for all-solid-state SnS2/Na batteries with excellent interfacial compatibility between electrolyte and Na metal, J. Energy Chem. 41 (2020) 73–78, https://doi.org/10.1016/j.jechem.2019.05.003.
- [148] Z. Dai, U. Mani, H.T. Tan, Q. Yan, Advanced cathode materials for sodium-ion batteries: what determines our choices, Small Methods 1 (5) (2017), 1700098, https://doi.org/10.1002/smtd.201700098.
- [149] Y. Yao, Z. Wei, H. Wang, H. Huang, Y. Jiang, X. Wu, X. Yao, Z.S. Wu, Y. Yu, Toward high energy density all solid-state sodium batteries with excellent flexibility, Adv. Energy Mater. 10 (12) (2020), https://doi.org/10.1002/ aenm.201903698.
- [150] Y. Ruan, F. Guo, J. Liu, S. Song, N. Jiang, B. Cheng, Optimization of Na3Zr2Si2PO12 ceramic electrolyte and interface for high performance solidstate sodium battery, Ceram. Int. 45 (2) (2019) 1770–1776, https://doi.org/ 10.1016/j.ceramint.2018.10.062.
- [151] P. Wen, P. Lu, X. Shi, Y. Yao, H. Shi, H. Liu, Y. Yu, Z.S. Wu, Photopolymerized gel electrolyte with unprecedented room-temperature ionic conductivity for high-

- energy-density solid-state sodium metal batteries, Adv. Energy Mater. (2020), https://doi.org/10.1002/aenm.202002930.
- [152] W.J. Li, C. Han, W. Wang, F. Gebert, S.L. Chou, H.K. Liu, X. Zhang, S.X. Dou, Commercial prospects of existing cathode materials for sodium ion storage, Adv. Energy Mater. 7 (24) (2017), https://doi.org/10.1002/aenm.201700274.
- [153] X. Yu, L. Xue, J.B. Goodenough, A. Manthiram, Ambient-temperature all-solid-state sodium batteries with a laminated composite electrolyte, Adv. Funct. Mater. 31 (2) (2021), https://doi.org/10.1002/adfm.202002144.
- [154] L. Duchêne, D.H. Kim, Y.B. Song, S. Jun, R. Moury, A. Remhof, H. Hagemann, Y. S. Jung, C. Battaglia, Crystallization of closo-borate electrolytes from solution
- enabling infiltration into slurry-casted porous electrodes for all-solid-state batteries, Energy Storage Mater. 26 (2020) 543–549, https://doi.org/10.1016/j.ensm.2019.11.027.
- [155] J.F. Wu, Z.Y. Yu, Q. Wang, X. Guo, High performance all-solid-state sodium batteries actualized by polyethylene Oxide/Na2Zn2TeO6 composite solid electrolytes, Energy Storage Mater. 24 (2020) 467–471, https://doi.org/10.1016/ ionep.2010.07.012
- [156] H. Gao, S. Xin, L. Xue, J.B. Goodenough, Stabilizing a high-energy-density rechargeable sodium battery with a solid electrolyte, Chem 4 (4) (2018) 833–844, https://doi.org/10.1016/j.chempr.2018.01.007.